

Two-Stage Estimators for Spatial Confounding

Nate Wiecha^{1,*}, Jane A. Hoppin², and Brian J. Reich¹

¹Department of Statistics, North Carolina State University, Raleigh, North Carolina, U.S.A

²Department of Biological Sciences, North Carolina State University, Raleigh, North Carolina, U.S.A

**email*: nbwiecha@ncsu.edu

SUMMARY: Public health data are often spatially dependent, but standard spatial regression methods can suffer from bias and invalid inference when the independent variable is associated with spatially-correlated residuals. This could occur if, for example, there is an unmeasured environmental contaminant associated with the independent and outcome variables in a spatial regression analysis. Geoadditve structural equation modeling (gSEM), in which an estimated spatial trend is removed from both the explanatory and response variables before estimating the parameters of interest, has previously been proposed as a solution, but there has been little investigation of gSEM's properties with point-referenced data. We link gSEM to results on double machine learning and semiparametric regression based on two-stage procedures. We propose using these semiparametric estimators for spatial regression using Gaussian processes with Matèrn covariance to estimate the spatial trends, and term this class of estimators Double Spatial Regression (DSR). We derive regularity conditions for root- n asymptotic normality and consistency and closed-form variance estimation, and show that in simulations where standard spatial regression estimators are highly biased and have poor coverage, DSR can mitigate bias more effectively than competitors and obtain nominal coverage.

KEY WORDS: Bias reduction, double machine learning, Gaussian process, semiparametric regression

1. Introduction

Public health data are often observational and exhibit spatial dependence, such as in environmental contaminations that may spread over a geographic region (Cressie, 1993). Spatial regression methods can improve efficiency, allow proper uncertainty quantification, and enhance predictive accuracy (Cressie, 1993). However, association between explanatory variables and latent functions of space in the response model can cause bias in estimated regression coefficients, and invalid statistical inference due to poor uncertainty quantification (Reich et al., 2006). This has often been termed “spatial confounding,” and was first observed in Clayton et al. (1993), discussed further in Reich et al. (2006) and Hodges and Reich (2010), and studied in other papers such as Paciorek (2010). The analogous issue in spline models has been discussed in Rice (1986) and Wood (2017). Several recent papers (Gilbert et al., 2021; Dupont et al., 2023; Khan and Berrett, 2023) have discussed definitions, causes, and effects of spatial confounding in attempts to unify varying accounts.

Methods proposed to deal with spatial confounding aim to reduce bias in linear regression parameter estimates, such as in Marques et al. (2022), Guan et al. (2022), and Schnell and Papadogeorgou (2020). Methods similar to our proposal are geoaddivitive structural equation modeling (Thaden and Kneib, 2018), Spatial+ (Dupont et al., 2022), and a shift estimand, which does not assume a linear treatment effect, studied in Gilbert et al. (2021). Geoaddivitive structural equation modeling (gSEM) subtracts estimated latent functions of space from the treatment and response, and regresses those residuals onto each other. Spatial+ subtracts an estimated function of space from the treatment variable and regresses the response onto those residuals. The shift estimand implemented in Gilbert et al. (2021) subtracts an estimated function of space from the treatment (in order to estimate a conditional density function) and response, but without assuming a linear and additive effect of the explanatory variable. Identifiability in gSEM, Spatial+, the shift estimand, and our method is typically due to

independent, non-spatial variation in the treatment and response. In this situation, Gilbert et al. (2023) also showed that the standard generalized least squares (GLS), spline, and Gaussian process estimates are consistent even in some cases where they are misspecified due to spatial confounding, but noted that this does not imply variance estimates are accurate, and these estimators may converge at a rate slower than $n^{-1/2}$.

gSEM was initially proposed for areal spatial data, and its analogue for point-referenced spatial data has not been studied thoroughly. The subject of this paper is point-referenced spatial data, so we use “gSEM” to refer to its implementation described above, not the version for areal data. Dupont et al. (2022) states that “it is not immediately clear why the method works”; Khan and Berrett (2023) states that “the GSEM approach will result in inference...equivalent to that of a non-spatial analysis using the originally observed [variables]”; Dupont et al. (2023) states that “the bias reduction will only be successful under the assumption that the initial regressions successfully remove all spatial confounders.” The gSEM estimator has also lacked a closed-form variance estimate.

Literature on semiparametric regression (Robinson, 1988; Andrews, 1994; Chernozhukov et al., 2018) proves that under spatial confounding and additional regularity conditions, a class of estimators, including some nearly identical to gSEM (Robinson, 1988), can achieve $n^{-1/2}$ -consistency and asymptotic normality, with a consistent closed-form variance estimate, even when not removing spatial confounding exactly in initial regression estimates of spatial trends. Broadly speaking, these estimators first estimate the latent functions of space using nonparametric regression, subtract these estimates from the observed variables, and use those residuals to obtain an estimate, $\hat{\beta}_0$, of the parameter of interest in a second stage; the preliminary estimates of the latent functions need converge to the true values only slowly. Due to a form of orthogonality between $\hat{\beta}_0$ and the preliminary estimates of the latent functions, the asymptotic variance of $\hat{\beta}_0$ is unaffected by the use of these preliminary

estimates. By either using sample-splitting as in Chernozhukov et al. (2018) or requiring additional smoothness conditions as in Andrews (1994), asymptotic bias due to overfitting is controlled. A more detailed overview in the Supplementary Materials section S1 draws heavily from Chernozhukov et al. (2018) and Andrews (1994).

We apply these semiparametric estimators to spatial confounding scenarios, using Gaussian Process (GP) regression to estimate the latent functions of space. We primarily rely on methods and theory from Chernozhukov et al. (2018). As the two-stage estimators are termed Double Machine Learning (DML) in Chernozhukov et al. (2018), we refer to their narrower use to address spatial confounding as Double Spatial Regression (DSR). In simulations of spatial confounding, we show that DSR can provide superior performance in severe confounding scenarios, and verify that gSEM can also provide a notable bias reduction over standard spatial and non-spatial regression. Finally, we analyze the association between five per- and polyfluoroalkyl substances (PFAS) and thyroid stimulating hormone (TSH) levels in blood using DSR.

2. Double Spatial Regression

For $i \in \{1, \dots, n\}$, let $Y_i \in \mathbb{R}$ be the response variable, $\mathbf{A}_i = (a_{i1}, a_{i2}, \dots, a_{i\ell})^T \in \mathbb{R}^\ell$ be the treatment variables, $\mathbf{Z}_i = (z_{i1}, z_{i2}, \dots, z_{iv})^T \in \mathbb{R}^v$ be the covariates, and \mathbf{S}_i be the spatial location contained in spatial domain $\mathcal{S} \subset \mathbb{R}^d$. The assumed model for $i = 1, \dots, n$ and $j = 1, \dots, \ell$ is:

$$\begin{aligned} Y_i &= \mathbf{A}_i^T \boldsymbol{\beta}_0 + \mathbf{Z}_i^T \boldsymbol{\theta}_{00} + g_0(\mathbf{S}_i) + U_i \\ A_{ij} &= \mathbf{Z}_i^T \boldsymbol{\theta}_{0j} + m_{0j}(\mathbf{S}_i) + V_{ij}, \end{aligned} \tag{1}$$

where $\boldsymbol{\beta}_0$ is the regression coefficient vector of interest. The vectors $\boldsymbol{\theta}_{00}, \dots, \boldsymbol{\theta}_{0\ell}$ and the vector of functions $\boldsymbol{\eta}_0 = (g_0, m_{01}, \dots, m_{0\ell})$ are all nuisance parameters. U_i and V_{ij} are error terms such that $E(U_i | \mathbf{A}_i, \mathbf{Z}_i, \mathbf{S}_i) = E(V_{ij} | \mathbf{Z}_i, \mathbf{S}_i) = 0$ and which may be dependent. Given

$\beta_0, \theta_{00}, \dots, \theta_{0\ell}, \eta_0$, we assume the observation vectors $\mathbf{W}_i = (Y_i, \mathbf{A}_i, \mathbf{Z}_i, \mathbf{S}_i) \stackrel{iid}{\sim} P$ for some joint probability distribution P . For the theoretical results below, we use a random spatial design, but our empirical results verify that the proposed method can perform well if the \mathbf{S}_i are defined deterministically. Assume \mathbf{Y} and the columns of \mathbf{A} are centered so their means are 0.

In the following sections, we describe methods with and without cross-fitting, which correspond to the methods in Chernozhukov et al. (2018) and Andrews (1994) respectively, applied to spatial regression. For cross-fitting, the full data set is randomly partitioned into K folds each of size $\frac{n}{K}$, assumed to be an integer. Let $f_i \in \{1, \dots, K\}$ denote the fold assignment of observation i . For $k = 1, \dots, K$, let $\mathbf{k} = \{i : f_i = k\}$ denote the set of indices assigned to fold k and $\mathbf{k}^C = \{i : f_i \neq k\}$ denote the set of indices assigned to the complement of fold k . Then, for example, $\mathbf{Y}_{\mathbf{k}}$ is the vector of elements of \mathbf{Y} assigned to the k th fold and $\mathbf{Y}_{\mathbf{k}^C}$ is the vector of elements of \mathbf{Y} not assigned to the k th fold. For a matrix $\mathbf{A} \in \mathbb{R}^{n \times p}$, the elements of the matrix in the i th row are denoted \mathbf{A}_i , elements in the j th column are denoted $\mathbf{A}_{.j}$, and the elements in the k th fold and the j th column are denoted $\mathbf{A}_{\mathbf{k},j}$. The number of elements in fold k is denoted by $|\mathbf{k}|$. Denote the full sample as \mathbf{W} , the data in fold k as $\mathbf{W}_{\mathbf{k}}$, and the data in the complement of fold k as $\mathbf{W}_{\mathbf{k}^C}$.

2.1 Double Spatial Regression estimator for theoretical analysis

In this section, we consider an algorithm similar to gSEM (Thaden and Kneib, 2018) and the estimator in Robinson (1988), which allows derivation of explicit regularity conditions. An alternative estimator which performs better in simulations, but is slightly less amenable to asymptotic analysis, is presented in Section 2.3. For theoretical analysis, we combine treatment variables \mathbf{A}_i and covariates \mathbf{Z}_i into a combined vector \mathbf{X}_i of regressors of length

p . The model considered is then, for $i = 1, \dots, n$ and $j = 1, \dots, p$:

$$\begin{aligned} Y_i &= \mathbf{X}_i^T \boldsymbol{\beta}_0 + g_0(\mathbf{S}_i) + U_i, & E(U_i | \mathbf{X}_i, \mathbf{S}_i) &= 0 \\ X_{ij} &= m_{0j}(\mathbf{S}_i) + V_{ij}, & E(V_{ij} | \mathbf{S}_i) &= 0. \end{aligned} \quad (2)$$

DSR uses Kriging (although other nonparametric estimators can be used) which requires a working correlation function be specified, and for theoretical analysis we use the Gaussian correlation function (Rasmussen and Williams, 2005):

$$C_\gamma(\mathbf{S}_i, \mathbf{S}_j) := \exp\left(-\frac{\|\mathbf{S}_i - \mathbf{S}_j\|_2^2}{\gamma^2}\right).$$

For matrix inputs \mathbf{A} and \mathbf{B} to a correlation function, $C(\mathbf{A}, \mathbf{B})$ denotes the correlation matrix where the element in row i and column j equals $C(\mathbf{A}_{i\cdot}, \mathbf{B}_{\cdot j})$.

Denote by $h_0(\mathbf{s})$ the conditional expectation $E(Y_i | \mathbf{S}_i = \mathbf{s})$ (note that this does not depend on \mathbf{X}_i). On each fold k , Kriging (Stein, 1999) is used to obtain cross-fitted estimates for $h_0(\mathbf{S}_{\mathbf{k}})$ and $m_{0j}(\mathbf{S}_{\mathbf{k}})$ for $j = 1, \dots, p$:

$$\hat{h}_0(\mathbf{S}_{\mathbf{k}}) := C_{\gamma_{0k}}(\mathbf{S}_{\mathbf{k}}, \mathbf{S}_{\mathbf{k}^c}) \left(C_{\gamma_{0k}}(\mathbf{S}_{\mathbf{k}^c}, \mathbf{S}_{\mathbf{k}^c}) + |\mathbf{k}^c| \lambda_{0k} \mathbf{I} \right)^{-1} \mathbf{Y}_{\mathbf{k}^c} \quad (3)$$

$$\hat{m}_{0j}(\mathbf{S}_{\mathbf{k}}) := C_{\gamma_{jk}}(\mathbf{S}_{\mathbf{k}}, \mathbf{S}_{\mathbf{k}^c}) \left(C_{\gamma_{jk}}(\mathbf{S}_{\mathbf{k}^c}, \mathbf{S}_{\mathbf{k}^c}) + |\mathbf{k}^c| \lambda_{jk} \mathbf{I} \right)^{-1} \mathbf{X}_{\mathbf{k}^c, j}. \quad (4)$$

Predictions are combined across folds to obtain $\hat{h}_0(\mathbf{S})$ and $\hat{m}_{01}(\mathbf{S}), \dots, \hat{m}_{0p}(\mathbf{S})$. The hyperparameters $\lambda_{0k}, \dots, \lambda_{pk}, \gamma_{0k}, \dots, \gamma_{pk}$ depend on k because our theoretical analysis requires that they are selected each time predictions are obtained (i.e., on each fold); they are selected using a training-validation split of $\mathbf{W}_{\mathbf{k}^c}$ (Eberts and Steinwart, 2013). The data in $\mathbf{W}_{\mathbf{k}^c}$ is split in two halves, a “training” half and a “validation” half. For each possible combination of hyperparameters (λ and γ) considered, the training half of $\mathbf{W}_{\mathbf{k}^c}$ is used to obtain predictions on the validation half of $\mathbf{W}_{\mathbf{k}^c}$. The pair of hyperparameters with lowest mean squared error (MSE) on the validation half of $\mathbf{W}_{\mathbf{k}^c}$ is selected for estimating η_0 evaluated at the locations corresponding to the data in $\mathbf{W}_{\mathbf{k}}$ (Eberts and Steinwart, 2013).

Letting $\hat{\mathbf{V}}_{\cdot j} = \mathbf{X}_{\cdot j} - \hat{m}_{0j}(\mathbf{S})$ and $\hat{U}_i = Y_i - \hat{h}_0(\mathbf{S}_i) - \hat{\mathbf{V}}_i^T \hat{\boldsymbol{\beta}}_0$, the DSR estimator and its

approximate variance are:

$$\hat{\beta}_0 = (\hat{\mathbf{V}}^T \hat{\mathbf{V}})^{-1} \hat{\mathbf{V}}^T (\mathbf{Y} - \hat{h}_0(\mathbf{S})) \quad (5)$$

$$\widehat{Var}(\hat{\beta}_0) = (\hat{\mathbf{V}}^T \hat{\mathbf{V}})^{-1} \sum_{i=1}^n \left[\hat{U}_i^2 \hat{\mathbf{V}}_i \hat{\mathbf{V}}_i^T \right] (\hat{\mathbf{V}}^T \hat{\mathbf{V}})^{-1}, \quad (6)$$

which are the estimators from Chernozhukov et al. (2018). The algorithm is presented in Algorithm 1. Note that this estimator is essentially the same as gSEM except that it uses sample splitting, the method of estimating the latent functions of space is not specified with gSEM, and gSEM has lacked a closed-form variance estimate; gSEM in turn is essentially identical to the estimator in Robinson (1988), except that Robinson (1988) uses nonparametric kernel regression estimators and provides a variance estimate.

2.2 Double Spatial Regression regularity conditions

Our theoretical analysis uses the results on convergence rates of GP regression from Eberts and Steinwart (2013) and asymptotic properties of DML estimators from Chernozhukov et al. (2018), which require fast-enough convergence of estimates of the latent functions, to obtain explicit regularity conditions on the latent functions of space h_0 and m_{01}, \dots, m_{0p} under which DSR is root- n asymptotically normal and consistent. The observations $\mathbf{W}_i = (Y_i, \mathbf{X}_i, \mathbf{S}_i)$ are assumed to be i.i.d. from a probability distribution P with density function $p(w)$, and for a function f , $\|f\|_{P,q} := \{\int |f(w)|^q p(w) dw\}^{1/q}$. The Euclidean norm is denoted $\|\cdot\|$, and $\|\cdot\|_p$ and $L_p(\mathbb{R}^d)$ are with respect to the Lebesgue measure.

As the assumptions govern the probability distribution P generating the i.i.d. random variables \mathbf{W}_i , for notational simplicity in the rest of this section, the subscript i is dropped. The assumptions for the DSR estimator obtained by Algorithm 1 are:

A1) The data are generated by (2).

A2) The errors U, \mathbf{V} are such that $E(U|\mathbf{X}, \mathbf{S}) = E(V_j|\mathbf{S}) = 0$, for $j = 1, \dots, p$, with $0 <$

$E(U^2|\mathbf{S}) \leq C$ and $0 < E(V_j^2|\mathbf{S}) \leq C$ for some constant $C > 0$ and all $\mathbf{S} \in \mathcal{S}$. Also,

Algorithm 1 Double Spatial Regression estimation of β_0 for theoretical study

Input: Centered response vector $\mathbf{Y} \in \mathbb{R}^n$, location matrix $\mathbf{S} \in \mathbb{R}^{n \times d}$, design matrix $\mathbf{X} \in \mathbb{R}^{n \times p}$

with centered columns.

Output: Estimate $\hat{\beta}_0$ of $\beta_0 \in \mathbb{R}^p$ and estimate $\widehat{Var}(\hat{\beta}_0)$ of $Var(\hat{\beta}_0) \in \mathbb{R}^{p \times p}$

Randomly partition the data into K folds so that the size of each fold is $\frac{n}{K}$.

for $k = 1, \dots, K$ **do**

Select the hyperparameters $\gamma_{0,k}, \lambda_{0,k} \in \mathbb{R}$ by a training-validation approach, using data in \mathbf{k}^C . The value of λ_{0k} is selected from an evenly-spaced grid of $\frac{1}{2n}$ values in $(0, 1]$, the lengthscale γ_{0k} is selected from an evenly-spaced grid of $\frac{1}{2n^{-1/4}}$ values in $(0, 1]$.

$$\hat{h}_0(\mathbf{S}_{\mathbf{k}}) \leftarrow C_{\gamma_{0k}}(\mathbf{S}_{\mathbf{k}}, \mathbf{S}_{\mathbf{k}^C}) \left(C_{\gamma_{0k}}(\mathbf{S}_{\mathbf{k}^C}, \mathbf{S}_{\mathbf{k}^C}) + |\mathbf{k}^C| \lambda_{0k} \mathbf{I} \right)^{-1} \mathbf{Y}_{\mathbf{k}^C}$$

for $j = 1, \dots, p$ **do**

Select the hyperparameters $\gamma_{j,k}, \lambda_{j,k} \in \mathbb{R}$ by a training-validation approach, using data in \mathbf{k}^C . The value of λ_{jk} is selected from an evenly-spaced grid of $\frac{1}{2n}$ values in $(0, 1]$, the lengthscale γ_{jk} is selected from an evenly-spaced grid of $\frac{1}{2n^{-1/4}}$ values in $(0, 1]$.

$$\hat{m}_{0j}(\mathbf{S}_{\mathbf{k}}) \leftarrow C_{\gamma_{jk}}(\mathbf{S}_{\mathbf{k}}, \mathbf{S}_{\mathbf{k}^C}) \left(C_{\gamma_{jk}}(\mathbf{S}_{\mathbf{k}^C}, \mathbf{S}_{\mathbf{k}^C}) + |\mathbf{k}^C| \lambda_{jk} \mathbf{I} \right)^{-1} \mathbf{X}_{\mathbf{k}^C, j}$$

end for

end for

Combine the predictions from each fold to obtain $\hat{h}_0(\mathbf{S}) \in \mathbb{R}^n$, $\hat{\mathbf{m}}_0(\mathbf{S}) \in \mathbb{R}^{n \times p}$

$$\hat{\mathbf{V}} \leftarrow \mathbf{X} - \hat{\mathbf{m}}(\mathbf{S})$$

$$\hat{\mathbf{J}} \leftarrow (\hat{\mathbf{V}}^T \hat{\mathbf{V}})^{-1}$$

$$\hat{\beta}_0 \leftarrow \hat{\mathbf{J}} \hat{\mathbf{V}}^T (\mathbf{Y} - \hat{h}_0(\mathbf{S}))$$

$$\widehat{Var}(\hat{\beta}_0) \leftarrow \hat{\mathbf{J}} \left(\sum_{i=1}^n \left[-\hat{\mathbf{V}}_i \hat{\mathbf{V}}_i^T \hat{\beta}_0 + \hat{\mathbf{V}}_i (Y_i - \hat{h}_0(\mathbf{S}_i)) \right]^2 \right) \hat{\mathbf{J}}^T$$

Return $\hat{\beta}_0, \widehat{Var}(\hat{\beta}_0)$

$E(U^2 \mathbf{V} \mathbf{V}^T)$ and $E(\mathbf{V} \mathbf{V}^T)$ have minimum eigenvalues bounded away from 0. The errors U and V_j are either contained in some interval or are normally distributed.

- A3) The spatial locations \mathbf{S} reside in a region \mathcal{S} contained in a $\|\cdot\|$ -unit ball in \mathbb{R}^d , and the boundary of \mathcal{S} has P -probability 0. The marginal distribution $P_{\mathcal{S}}$ of \mathbf{S} (derived from P) is absolutely continuous on \mathcal{S} and has a density $p_{\mathcal{S}} \in L_q(\mathbb{R}^d)$ for some $q \geq 1$.
- A4) If U is bounded, then h_0 is such that $Y \in [-M_0, M_0]$ for some $M_0 > 0$, and if U is normally distributed then $h_0 \in [-1, 1]$. Similarly, if V_j is bounded, then m_{0j} is such that $X_j \in [-M_j, M_j]$ for some $M_j > 0$, and if V_j is normally distributed then $m_{0j} \in [-1, 1]$, for $j = 1, \dots, p$.
- A5) The estimates $\hat{h}_0, \hat{m}_{01}, \dots, \hat{m}_{0p}$ are obtained using GP regression as described in Eberts and Steinwart (2013). The function \hat{h}_0 is clipped so that if U is bounded, $|\hat{h}_0| \leq M_0$ and if U is normally distributed, $|\hat{h}_0| \leq \min\{1, 4\sqrt{C_0}\sqrt{\ln(n)}\}$ for some $C_0 > 0$ that exceeds $\text{Var}(U|\mathbf{S}) \forall \mathbf{S} \in \mathcal{S}$. Similarly, for $j = 1, \dots, p$, \hat{m}_{0j} is clipped so that if V_j is bounded, $|\hat{m}_{0j}| \leq M_j$ and if V_j is normally distributed, $|\hat{m}_{0j}| \leq \min\{1, 4\sqrt{C_j}\sqrt{\ln(n)}\}$ for some $C_j > 0$ that exceeds $\text{Var}(V_j|\mathbf{S}) \forall \mathbf{S} \in \mathcal{S}$.
- A6) For $j = 1, \dots, p$, the functions m_{0j} reside in the Besov space $B_{2s, \infty}^{\alpha_X}$ where the smoothness order $\alpha_X > \frac{d}{2}$, $\alpha_X \geq 1$, and $\frac{1}{s} + \frac{1}{q} = 1$ and $s \geq 1$, and h_0 resides in the Besov space $B_{2s, \infty}^{\alpha_Y}$ where the smoothness order $\alpha_Y > \frac{d^2}{4\alpha_X}$ and $\alpha_Y \geq 1$. Furthermore, $h_0, m_{01}, \dots, m_{0p} \in L_2(\mathbb{R}^d) \cap L_{\infty}(\mathbb{R}^d)$.

In the common scenario $d = 2$, a stronger but more interpretable alternative to Assumption A6 is that $h_0, m_{01}, \dots, m_{0p}$ are each in $L_2(\mathbb{R}^d) \cap L_{\infty}(\mathbb{R}^d)$, each has at least two (weak) derivatives, and these functions and derivatives are all in $L_{2s}(\mathbb{R}^d)$; further explanation of the smoothness conditions are in the Supplementary Materials Section S2. Per the discussion following Theorem 3.6 in Eberts and Steinwart (2013), U, V_1, \dots, V_p can follow other light-tailed distributions aside from normal.

Theorem 1 states that the DSR estimator in (5) is root- n asymptotically normal and consistent under the above assumptions.

THEOREM 1: *If Assumptions A1 – A6 are met, and $\hat{\boldsymbol{\beta}}_0$ and $\widehat{Var}(\hat{\boldsymbol{\beta}}_0)$ are obtained by Algorithm 1, then*

$$\begin{aligned}\sqrt{n}\boldsymbol{\Sigma}^{-1/2}(\hat{\boldsymbol{\beta}}_0 - \boldsymbol{\beta}_0) &\xrightarrow{D} N(\mathbf{0}, \mathbf{I}_p), \text{ and} \\ \widehat{Var}(\hat{\boldsymbol{\beta}}_0)^{-1/2}(\hat{\boldsymbol{\beta}}_0 - \boldsymbol{\beta}_0) &\xrightarrow{D} N(\mathbf{0}, \mathbf{I}_p),\end{aligned}$$

where $\boldsymbol{\Sigma} = E[\mathbf{V}\mathbf{V}^T]^{-1}E[U^2\mathbf{V}\mathbf{V}^T](E[\mathbf{V}\mathbf{V}^T]^{-1})$ is the approximate variance of $\hat{\boldsymbol{\beta}}_0$.

The proof of Theorem 1 is in the Supplementary Materials Section S6.

2.3 Practical modifications to Double Spatial Regression

In this section, we propose an alternative DSR estimator that is more practical than that of Section 2.1, although it lacks equally explicit regularity conditions. The previous estimator does not differentiate between treatment variables and covariates, combines the latent functions of space into the conditional expectation $h_0(\mathbf{s}) = E(Y_i|\mathbf{S}_i = \mathbf{s})$ which in simulations appears to cause performance to suffer, and uses a nonparametric GP regression method that has middling performance in finite samples despite its asymptotic performance guarantees. Finally, cross-fitting may not be desirable in some circumstances, and an estimator without cross-fitting as in Andrews (1994) is also considered in this section.

For our practical estimator, we use the Matèrn correlation function which may provide better estimates of rough functions (Stein, 1999). The Matèrn correlation function is:

$$C_{\gamma,\tau}(\mathbf{S}_i, \mathbf{S}_j) := \frac{2^{1-\tau}}{\Gamma(\tau)} \left(\sqrt{2\tau} \frac{\|\mathbf{S}_i - \mathbf{S}_j\|_2}{\gamma} \right)^\tau K_\tau \left(\sqrt{2\tau} \frac{\|\mathbf{S}_i - \mathbf{S}_j\|_2}{\gamma} \right), \quad (7)$$

where K_τ is the modified Bessel function of the second kind. The Matèrn correlation function has two hyperparameters: γ controls the range of spatial dependence and τ controls the smoothness of the process. A variance parameter ω^2 is typically defined so that $\omega^2 C(\mathbf{A}, \mathbf{B})$ is a covariance matrix.

Universal Kriging (Stein, 1999) is used to estimate $g_0, m_{01}, \dots, m_{0\ell}$. Unlike in Sections 2.1 and 2.2, the covariates \mathbf{Z} are separated from \mathbf{A} and incorporated into the prediction models

for $\mathbf{Y}, \mathbf{A}_1, \dots, \mathbf{A}_p$. If cross-fitting is used, the equations on fold k are:

$$\hat{g}_0(\mathbf{S}_{\mathbf{k}}) = \hat{\omega}_{0k} C_{\hat{\gamma}_{0k}, \hat{\tau}_{0k}}(\mathbf{S}_{\mathbf{k}}, \mathbf{S}_{\mathbf{k}^c}) \left(\hat{\omega}_{0k} C_{\hat{\gamma}_{0k}, \hat{\tau}_{0k}}(\mathbf{S}_{\mathbf{k}^c}, \mathbf{S}_{\mathbf{k}^c}) + \hat{\sigma}_{0k}^2 \mathbf{I} \right)^{-1} \quad (8)$$

$$\times (\mathbf{Y}_{\mathbf{k}^c} - \mathbf{A}_{\mathbf{k}^c}^T \hat{\boldsymbol{\beta}}_{0k} - \mathbf{Z}_{\mathbf{k}^c}^T \hat{\boldsymbol{\theta}}_{0k})$$

$$\hat{m}_{0j}(\mathbf{S}_{\mathbf{k}}) = \hat{\omega}_{jk} C_{\hat{\gamma}_{jk}, \hat{\tau}_{jk}}(\mathbf{S}_{\mathbf{k}}, \mathbf{S}_{\mathbf{k}^c}) \left(\hat{\omega}_{jk} C_{\hat{\gamma}_{jk}, \hat{\tau}_{jk}}(\mathbf{S}_{\mathbf{k}^c}, \mathbf{S}_{\mathbf{k}^c}) + \hat{\sigma}_{0j}^2 \mathbf{I} \right)^{-1} (\mathbf{A}_{\mathbf{k}^c, j} - \mathbf{Z}_{\mathbf{k}^c}^T \hat{\boldsymbol{\theta}}_{jk}), \quad (9)$$

for $j = 1, \dots, p$. Note that $\tilde{\boldsymbol{\beta}}_0$ is a preliminary estimate of $\boldsymbol{\beta}_0$ only. For this working prediction model we also assume homoskedasticity of all error terms, with variance parameters $\sigma_0^2, \sigma_1^2, \dots, \sigma_\ell^2$, and we also include the variance of the spatial processes $\omega_0^2, \omega_1^2, \dots, \omega_\ell^2$. To obtain universal Kriging estimates, we used the `GpGp` R package (Guinness, 2018), which estimates all covariance and slope parameters using restricted maximum likelihood (REML) and the full data set, and the Vecchia approximation (Vecchia, 1988), and scales well to large sample sizes. As before estimates are combined across folds to obtain $\hat{g}_0(\mathbf{S})$ and $\hat{m}_{01}(\mathbf{S}), \dots, \hat{m}_{0p}(\mathbf{S})$. If cross-fitting is not used, all subsets of the data in (8) and (9) are replaced by the full sample.

If cross-fitting is used, different random allocations of observations into folds will produce different estimates of $\boldsymbol{\beta}_0$. For a scalar β_0 , Fuhr et al. (2024) recommends using enough folds that the estimates are relatively stable, and pick the median point and variance estimates out of as large a number of estimates as is feasible. The marginal median could be selected for each component of $\hat{\boldsymbol{\beta}}_0$ if it has length greater than 1.

The expressions for the estimator and its variance estimate are the same with and without cross-fitting. Letting $\hat{\mathbf{V}}_{\cdot j} = \mathbf{A}_j - \hat{m}_{0j}(\mathbf{S})$, $\hat{U}_i = Y_i - \mathbf{A}_i^T \hat{\boldsymbol{\beta}}_{DSR} - \mathbf{Z}_i^T \hat{\boldsymbol{\theta}}_0 - \hat{g}_0(\mathbf{S}_i)$, and $\hat{\mathbf{J}} = (\hat{\mathbf{V}}^T \mathbf{A})^{-1}$:

$$\hat{\boldsymbol{\beta}}_{DSR} = \hat{\mathbf{J}} \hat{\mathbf{V}}^T (\mathbf{Y} - \mathbf{Z}^T \hat{\boldsymbol{\theta}}_0 - \hat{g}_0(\mathbf{S})) \quad (10)$$

$$\widehat{Var}(\hat{\boldsymbol{\beta}}_{DSR}) = \hat{\mathbf{J}} \left(\sum_{i=1}^n \hat{U}_i^2 \hat{\mathbf{V}}_i \hat{\mathbf{V}}_i^T \right) \hat{\mathbf{J}}^T, \quad (11)$$

which are the estimators provided in Chernozhukov et al. (2018).

Root- n consistency of $\hat{\beta}_{DSR}$ and asymptotic normality of $\widehat{Var}(\hat{\beta}_{DSR})^{-1/2}(\hat{\beta}_{DSR} - \beta_0)$ require convergence of the estimates from (8) and (9) at rates of $o_P(n^{-1/4})$, along with correct model specification and further standard regularity conditions (Chernozhukov et al., 2018). Andrews (1994) provides sufficient conditions to forego cross-fitting, namely that both $\eta_0 = (g_0, m_{01}, \dots, m_{0p})$ and $\hat{\eta}_0$ obey additional smoothness conditions. These required results for GP regression with Matèrn correlation and hyperparameters estimated via REML are not established to our knowledge, so this DSR estimator could be used, and cross-fitting could be skipped if desired, with assumptions about both η_0 and $\hat{\eta}_0$.

Detailed algorithms for the estimators in this section are in the Supplementary Materials Section S3.

3. Simulation Study

3.1 Simulation study outline

In this simulation study, we evaluate several estimators' performance in finite samples. We include the DSR estimator presented in Section 2.3 (Equations 10 and 11), which we refer to as “DSR” in this section, and the “theoretical DSR” estimator studied in Section 2.1 (Algorithm 1). Cross-fitting is used for all DSR results presented in this section; the Supplementary Materials Section S5 include results for both versions of DSR without cross-fitting. For theoretical DSR, we use a grid of possible γ values of size $\frac{1}{2n^{-1/2}}$ to improve finite-sample performance. DSR estimators with cross-fitting used $K = 5$ folds. We also implemented DSR without cross-fitting and using spline regression to estimate latent functions of space, to isolate differences with gSEM. Comparison methods were the geoaddivitive structural equation model (gSEM) of Thaden and Kneib (2018), implemented using splines for geostatistical data (similar to Algorithm 1, but using spline regression instead of GP regression, and without cross-fitting; see the Supplementary Materials Section S3), Spatial+ of Dupont et al. (2022),

the naive (unadjusted for spatial confounding) spatial linear mixed model (LMM), spline regression using generalized cross-validation (GCV) and REML to estimate the smoothing parameter for a smooth function of space (Wood, 2017), and ordinary least squares (OLS). The nonparametric shift estimator studied in Gilbert et al. (2021) was tried but was not able to obtain estimates in most scenarios we used. Spatial+ removes a fitted spatial surface from the treatment variable, and then performs thin-plate spline regression of the outcome onto the residuals. The naive spatial linear mixed model (LMM) is fitted using the R package `GpGp` (Guinness, 2018) and spline models fit using the R package `mgcv` (Wood, 2011). Simulations were carried out in R version 4.2.1 (R Core Team, 2023).

3.2 Data generating process

For our main simulations, we generate data from Gaussian processes in order to control the smoothness of the generated processes. Observations were drawn from multivariate normal distributions with selected covariances, equivalent to drawing a random function from a Gaussian process prior with that kernel. The data-generating process for the main simulations is similar to that used in Marques et al. (2022):

$$\mathbf{Y} \sim N(\beta_0 \mathbf{A} + \mathbf{U}, \sigma_Y^2 \mathbf{I})$$

$$\begin{bmatrix} \mathbf{A} \\ \mathbf{U} \end{bmatrix} \sim N \left(\begin{bmatrix} \mathbf{0} \\ \mathbf{0} \end{bmatrix}, \begin{bmatrix} \Sigma_{\mathbf{A}} + \sigma_A^2 \mathbf{I} & \rho \Sigma_{\mathbf{A}}^{1/2} (\Sigma_{\mathbf{U}}^{1/2})^T \\ \rho \Sigma_{\mathbf{U}}^{1/2} (\Sigma_{\mathbf{A}}^{1/2})^T & \Sigma_{\mathbf{U}} \end{bmatrix} \right),$$

where $\mathbf{Y}, \mathbf{A}, \mathbf{U} \in \mathbb{R}^n$, $\Sigma_{\mathbf{A}}$ and $\Sigma_{\mathbf{U}}$ are spatial correlation matrices in $\mathbb{R}^{n \times n}$, and $\rho \in [-1, 1]$.

\mathbf{A} is the independent variable, β_0 is the parameter of interest, and \mathbf{U} is an unobserved confounder. We used two spatial covariance matrices for both $\Sigma_{\mathbf{A}}$ and $\Sigma_{\mathbf{U}}$ that generate realizations of smooth and rough functions of space:

- Rough: Matèrn covariance function with smoothness parameter $\tau = 1.5$, range parameter $\gamma = 0.2$, and variance 1

- Smooth: Gneiting covariance function (Schlather et al., 2015) with range parameter $\gamma = 0.2$, and variance 1

The Gneiting covariance function approximates a Gaussian covariance function but is less prone to producing computationally singular covariance matrices (Schlather et al., 2015). These were both used as implemented in the R package `geoR` (Ribeiro Jr et al., 2023).

For our main simulations, $n = 1000$, $\rho = 0.5$, $\sigma_A^2 = 0.1^2$, $\sigma_Y^2 = 1$, and $\beta_0 = 0.5$. The relative lack of i.i.d. variance in \mathbf{A} provides less unconfounded variation in the treatment, causing severe spatial confounding bias in finite samples. Spatial locations were randomly sampled uniformly from $[0, 1]^2$. Several additional simulated scenarios generated data subject to heteroskedasticity, nonstationarity, non-Gaussianity of the confounder U_i or noise ϵ_i , or considering deterministically-defined latent functions of space g_0 and m_0 as in (2) rather than random functions drawn from GP priors. These scenarios are discussed in the Supplementary Materials Section S4.

Four hundred Monte Carlo replications were performed for each main simulation scenario. Confidence intervals for Spatial+ and gSEM were obtained using 100 nonparametric bootstrap replicates. No adjustment was made in the bootstrapping procedure for spatial correlation between observations, or the tendency of GAMs to under-smooth in bootstrap samples described in Wood (2017). Spline models, gSEM, and Spatial+ used 300 spline basis functions. Methods were compared using their bias, standard error, mean squared error (MSE), coverage, and confidence interval length.

3.3 Simulation results

Figure 1 displays sampling distributions of $\hat{\beta}_0 - \beta_0$ for several scenarios and a subset of methods. Table S1 displays corresponding coverage and mean confidence interval lengths. DSR has the lowest bias and shortest confidence intervals of the methods with at least near-nominal coverage. Theoretical DSR performs fairly poorly in terms of bias, coverage, and

confidence interval length. gSEM and Spatial+ are improvements over the linear mixed model, and achieve nominal coverage, but they have higher bias and wider confidence intervals than DSR. These scenarios were chosen to be particularly challenging cases of spatial confounding, so the linear mixed model performs poorly by all metrics.

[Figure 1 about here.]

[Table 1 about here.]

Full simulation result tables are in the Supplementary Material Section S5, tables S1-S13. These include the non-Gaussian/non-stationary scenarios, in which DSR continued to perform well. In some scenarios, especially the deterministic scenarios where the latent functions of space were predefined, using cross-fitting reduced bias and improved coverage of the DSR estimators. DSR implemented with spline regression without cross-fitting outperformed gSEM in many scenarios, indicating that direct estimation of $g_0(\mathbf{S})$ rather than $h_0(\mathbf{S})$, which marginalizes over the distribution of \mathbf{A} , generally improves performance. In the two deterministic scenarios, gSEM is slightly preferred when $g_0 = m_0$, but DSR is slightly preferred when $g_0 \neq m_0$, perhaps confirming that DSR's strength is in its estimate of the separate spatial trends. In the deterministic scenarios performance suffered relative to the scenarios with randomly-drawn functions of space, although the deterministic scenarios likely correspond to more severe confounding scenarios—the LMM's estimated bias in the deterministic scenarios was about twice its estimated bias in other scenarios.

The confounding scenario in which \mathbf{A} and \mathbf{U} were generated with exponential covariance proved too difficult for any method to perform well and all suffered from substantial bias (Table S10 in the Supplementary Materials). Among the scenarios in which an adjustment for spatial confounding appeared possible, the ones in which DSR appeared to have some disadvantage was when both \mathbf{A} and \mathbf{U} were both generated from rough spatial processes; when $\sigma_A^2 = 1$; and when \mathbf{U} was cubed; in which DSR had slightly lower-than-nominal

coverage. When $\sigma_A^2 = 1$, DSR also had higher bias than gSEM and the shift estimand, although all methods had low bias in this scenario. In the deterministic scenarios, in which DSR with cross-fitting suffered from coverage of about 0.80 in the first deterministic scenario and about 0.90 in the second, with somewhat worse coverage for the estimator without sample-splitting, although bias was competitive with or better than other methods.

4. PFAS Data Analysis

Per- and polyfluoroalkyl substances (PFAS) are synthetic chemicals resistant to water and stains used in consumer products and manufacture of chemicals, many of which are frequently detected in humans due to resistance to degradation and solubility in water (National Academies of Sciences, Engineering, and Medicine, 2022). In Sun et al. (2016), high concentrations of a number of PFAS were detected in water at several collection points of the Cape Fear River in North Carolina (NC), the drinking water source for over a million people. One source of contamination is a fluorochemical manufacturing plant slightly downstream of Fayetteville, North Carolina (Kotlarz et al., 2020, 2024). In 2017, the GenX Exposure Study began collecting data on North Carolina residents in drinking water exposed communities in order to understand their patterns of exposure to PFAS and possible health effects. The data used in this analysis comes from blood samples collected from study participants in the private well community near the chemical plant in October 2021. We study associations between five PFAS, because each was detected in at least 80% of our samples, and thyroid stimulating hormone (TSH).

The sample from this community is comprised of 98 adult women who obtain their water from private wells, who lived near the Fayetteville chemical plant, and who did not have thyroid disease at the time of data collection. Women with thyroid disease were excluded because thyroid medication can stabilize thyroid hormone levels. The outcome variable we studied was blood serum concentration of TSH. We focus on this outcome and community because

the geographic area was relatively small (about 250 square miles), and the outcome and some exposures showed spatial dependence, so this analysis is a candidate for a spatial confounding adjustment. For example, other unmeasured pollutants might affect health outcomes and be correlated with the PFAS used in the analysis due to similar sources or spread. Our sample size is small, but we believe it is reasonable to assume that geographic distributions of these environmental contaminants are smooth, in which scenario DSR performed well even with very high levels of confounding in the simulation study. TSH was log-transformed to obtain approximately normal residuals. The data underlying this article cannot be shared publicly, for the privacy of individuals that participated in the study. The data will be shared on reasonable request to the corresponding author.

National Academies of Sciences, Engineering, and Medicine (2022) “concluded that there is limited or suggestive evidence of an association between PFAS and thyroid hormones and thyroid disease.” Further studies are needed to understand the possible association in humans between PFAS exposure and thyroid function. Double spatial regression may offer an improved ability to analyze the effects of spatially-correlated chemical exposures, which may otherwise be difficult to estimate without adjustment for spatial confounding in standard models.

Exposure variables were serum concentrations of five different PFAS detected in more than 80% of our sample: PFHpS, PFOA, PFNA, PFOS, and PFHxS. The blood serum concentrations of PFAS and thyroid hormones were measured in the same samples. Wallis et al. (2023) summarizes results from Li et al. (2018), Li et al. (2022), and Zhang et al. (2013) that show fairly long half-lives of these chemicals, indicating that the measurements taken for these PFAS are good proxies of cumulative exposure. We controlled for several confounders that could be associated with both exposures and outcome: age, sex, race, smoking status and current alcohol consumption. Table S2 provides summary statistics of the continuous

variables. Thirty-nine members (40%) of the sample had ever smoked, forty-two members (43%) currently drank, and 78 (80%) were White, ten (10%) were Black, and ten (10%) were other or multiple races. The median age was 59 years, with a mean of 56.9 and standard deviation of 14.7.

We estimated the joint associations between the five PFAS and TSH using non-spatial linear regression, a spatial linear mixed model (LMM) estimated with `GpGp` using Matèrn covariance, `gSEM`, `Spatial+`, and the DSR estimator with cross-fitting in Section 2.3. A large number of folds, 45, was used in the DSR estimator to improve stability of estimates across random splits; the marginal median estimates, and corresponding variance estimates, were chosen from 11 runs with different random sample splits. Linear regression diagnostics showed that an assumption of a linear association of all PFAS serum concentrations with TSH was reasonable.

[Table 2 about here.]

Table S3 presents results using each method aside from `Spatial+`, which had essentially the same results as `gSEM`. Results were fairly consistent across spatial regression methods. The only PFAS found to be statistically significantly associated (at the 0.05 level) with the outcome variable was PFOS, which was found by all methods.

OLS (without a spatial term) found different results for several PFAS. The estimate for PFNA from OLS is lower than all of the spatial models. The OLS estimate for PFHpS is also lower in magnitude than the estimates yielded by the spatial models, and has a correspondingly lower t-value. While these other estimates do not cross the threshold of statistical significance with any method, modeling spatial correlation likely improves estimates. `gSEM` and `Spatial+` also have higher uncertainty in their estimates of PFHpS than OLS, LMM, or DSR, and the DSR estimate is larger in magnitude than that of the others. We also analyzed

these data using DSR without cross-fitting, which yielded more extreme results. Since using cross-fitting has greater theoretical justification, we only present those results.

[Table 3 about here.]

While analyzing the PFAS jointly provides mutually-adjusted estimates for each PFAS, it may increase variance of the estimates due to collinearity and possibly amplify left-out variable bias (Weisskopf et al., 2018), so Table S4 presents the results of analyzing each PFAS one at a time using DSR, again using 11 sample splits and selecting the median point estimate and corresponding variance estimate. The results are mostly similar from those in the joint analysis—PFNA, PFOA, and PFHxS now have even weaker associations with TSH, but the broad conclusions are the same.

[Table 4 about here.]

5. Discussion

Double spatial regression (DSR) is a method to estimate linear regression coefficients using point-referenced data that may be spatially confounded. In simulated confounding scenarios in which standard spatial regression models suffered from high bias and low coverage, DSR greatly reduced bias, typically achieved nominal or near-nominal coverage, and with the exception of under-coverage in some scenarios and inability of any method to perform well in scenarios with very rough spatial confounders, outperformed other competing methods in many scenarios. We derived explicit regularity conditions that govern asymptotic performance of a slightly different DSR estimator. These regularity conditions are fairly unrestrictive but this “theoretical DSR” estimator performed poorly in simulations with finite samples and severe confounding. DSR also allows closed-form variance estimation, which many competing methods have lacked. Cross-fitting appeared important to bias and coverage

particularly in confounding scenarios that appeared most difficult. Based on simulation results, our recommendation is to use the DSR estimator from Section 2.3 with cross-fitting.

We linked the problem of spatial confounding to existing results in the semiparametric regression literature, which has provided insight into why gSEM is able to reduce bias compared to the naive spatial linear mixed model, and studied Double Machine Learning estimators (which we termed Double Spatial Regression in our narrower application) that outperform others proposed so far. These existing results explain when and why these types of two-stage estimators are able to correct for bias, even when the initial nonparametric regression estimates converge to the true functions slowly. Our results differ from some of those of Khan and Berrett (2023), who found no bias reduction from gSEM compared to the LMM. One possible cause may be the simulation settings used. The exponential covariance used in the simulations of Khan and Berrett (2023) when generating spatially-correlated data results in very rough sample paths, and makes adjusting for resulting confounding bias very difficult. In our simulations using somewhat smoother latent functions of space, both gSEM and DSR improve inference over the LMM. With exponential covariances, no adjustment performed well (Table S10 in the Supplementary Materials), and gSEM had worse bias than the LMM, although DSR did not. Simulation results indicate that both use of GP regression using Matèrn covariance, and direct estimation of the function g_0 , as opposed to h_0 , which marginalizes over the distribution of A_i , reduced DSR’s bias compared to gSEM in many scenarios.

DSR is similar in some ways to the method studied in Gilbert et al. (2021), which used a double machine learning-based estimator to nonparametrically estimate the average effect of a shift in a treatment variable under spatial confounding, using bootstrapping to estimate variance. This shift estimator was well-suited to estimating the average treatment effect when treatment effects were heterogeneous. In many practical situations there are

multiple treatment variables, and it is reasonable to assume a linear and additive association between treatment(s) and response. In this situation, DSR is able to estimate multiple linear regression coefficients jointly, with their covariance matrix in closed-form, and with somewhat less variance and MSE than a strictly nonparametric estimate as in Gilbert et al. (2021) (Table S9 in the Supplementary Materials). The shift estimator exhibited lower bias than DSR in this scenario, but DSR and most methods exhibited low bias in this case. Gilbert et al. (2021) assumed increasing-domain asymptotics, while we assumed a fixed spatial domain.

Gilbert et al. (2021) also suggested using spatially-independent sample splits for cross-fitting, under an assumption of local spatial covariance. With this type of sample splitting, the conditional mean or density functions of the response and treatment variables, conditional on spatial location, are estimated using points in one subset of the spatial domain, and those functions' realized values estimated on a different subset of the spatial domain such that the points in the prediction set are spatially independent from the points in the training set. It is not clear that these estimates can converge to their true values when the training and prediction sets are spatially independent, since the goal is to learn functions of space; deriving conditions on the covariance functions generating the spatially-dependent data that are sufficient to achieve root- n asymptotic normality and consistency when using spatially-independent splits could verify when this strategy can be used.

Further research could analyze convergence rates of functions estimated with Gaussian processes, when hyperparameters are selected using maximum likelihood or REML rather than training-validation splits; the only work we are aware of doing this, although with noiseless observations, is Karvonen et al. (2020). This would help yield more explicit regularity conditions for the main DSR estimator we proposed (although we also proposed using the Vecchia approximation to the full likelihood). DSR could also be extended to use estimating equations of the type proposed by Robins et al. (2017), which require even less regularity of

the latent functions. Approaches to areal data should also be investigated. Finally, extensions to other types of semiparametric models, including weighted and nonlinear regression, are discussed in Robinson (1988), Andrews (1994), and Chernozhukov et al. (2018).

ACKNOWLEDGEMENTS

Nate Wiecha is supported by the GenX Exposure study, on United States National Institutes of Health Superfund grant number P42 ES031009. The GenX Exposure Study is supported by research funding from the National Institute of Environmental Health Sciences (1R21ES029353), Center for Human Health and the Environment (CHHE) at NC State University (P30 ES025128), the Center for Environmental and Health Effects of PFAS (P42 ES0310095), and the NC Policy Collaboratory. This work was also supported by National Institutes of Health grants R01ES031651-03 and NIH R01ES031651-01, and National Science Foundation grant DMS2152887. The views expressed in this manuscript are those of the authors and do not necessarily represent the views or policies of the National Institutes of Health.

REFERENCES

- Andrews, D. W. K. (1994). Asymptotics for semiparametric econometric models via stochastic equicontinuity. *Econometrica* **62**, 43–72.
- Belloni, A., Chernozhukov, V., Fernández-Val, I., and Hansen, C. (2017). Program evaluation and causal inference with high-dimensional data. *Econometrica* **85**, 233–298.
- Chernozhukov, V., Chetverikov, D., Demirer, M., Duflo, E., Hansen, C., Newey, W., and Robins, J. (2018). Double/debiased machine learning for treatment and structural parameters. *The Econometrics Journal* **21**, C1–C68.
- Chipman, H. A., George, E. I., and McCulloch, R. E. (2010). BART: Bayesian additive regression trees. *The Annals of Applied Statistics* **4**, 266 – 298.

- Clayton, D. G., Bernardinelli, L., and Montomoli, C. (1993). Spatial correlation in ecological analysis. *International Journal of Epidemiology* **22**, 1193–1202.
- Cressie, N. A. (1993). *Statistics for Spatial Data*. Wiley, 2nd edition.
- Dorie, V. (2024). *dbarts: Discrete Bayesian Additive Regression Trees Sampler*. R package version 0.9-26.
- Dupont, E., Marques, I., and Kneib, T. (2023). Demystifying spatial confounding. *arXiv preprint arXiv:2309.16861* .
- Dupont, E., Wood, S. N., and Augustin, N. H. (2022). Spatial+: A novel approach to spatial confounding. *Biometrics* **78**, 1279–1290.
- Eberts, M. and Steinwart, I. (2013). Optimal regression rates for SVMs using Gaussian kernels. *Electronic Journal of Statistics* **7**, 1 – 42.
- Fuhr, J., Berens, P., and Papias, D. (2024). Estimating causal effects with double machine learning—a method evaluation. *arXiv preprint arXiv:2403.14385* .
- Gilbert, B., Datta, A., Casey, J. A., and Ogburn, E. L. (2021). A causal inference framework for spatial confounding. *arXiv preprint arXiv:2112.14946* .
- Gilbert, B., Ogburn, E. L., and Datta, A. (2023). Consistency of common spatial estimators under spatial confounding. *arXiv preprint arXiv:2308.12181* .
- Guan, Y., Page, G. L., Reich, B. J., Ventrucci, M., and Yang, S. (2022). Spectral adjustment for spatial confounding. *Biometrika* **110**, 699–719.
- Guinness, J. (2018). Permutation and grouping methods for sharpening Gaussian Process approximations. *Technometrics* **60**, 415–429. PMID: 31447491.
- Hodges, J. S. and Reich, B. J. (2010). Adding spatially-correlated errors can mess up the fixed effect you love. *The American Statistician* **64**, 325–334.
- Huiying Mao, R. M. and Reich, B. J. (2023). Valid model-free spatial prediction. *Journal of the American Statistical Association* **0**, 1–11.

- Kanagawa, M., Hennig, P., Sejdinovic, D., and Sriperumbudur, B. K. (2018). Gaussian processes and kernel methods: A review on connections and equivalences. *arXiv preprint arXiv:1807.02582*.
- Karvonen, T., Wynne, G., Tronarp, F., Oates, C., and Särkkä, S. (2020). Maximum likelihood estimation and uncertainty quantification for Gaussian Process approximation of deterministic functions. *SIAM/ASA Journal on Uncertainty Quantification* **8**, 926–958.
- Khan, K. and Berrett, C. (2023). Re-thinking spatial confounding in spatial linear mixed models. *arXiv preprint arXiv:2301.05743*.
- Kotlarz, N., Guillette, T., Critchley, C., Collier, D., Lea, C. S., McCord, J., Strynar, M., Cuffney, M., Hopkins, Z. R., Knappe, D. R., and Hoppin, J. A. (2024). Per- and polyfluoroalkyl ether acids in well water and blood serum from private well users residing by a fluorochemical facility near Fayetteville, North Carolina. *Journal of Exposure Science & Environmental Epidemiology* **34**, 97–107.
- Kotlarz, N., McCord, J., Collier, D., Lea, C. S., Strynar, M., Lindstrom, A. B., Wilkie, A. A., Islam, J. Y., Matney, K., Tarte, P., et al. (2020). Measurement of novel, drinking water-associated PFAS in blood from adults and children in Wilmington, North Carolina. *Environmental Health Perspectives* **128**, 077005.
- Li, Y., Andersson, A., Xu, Y., Pineda, D., Nilsson, C. A., Lindh, C. H., Jakobsson, K., and Fletcher, T. (2022). Determinants of serum half-lives for linear and branched perfluoroalkyl substances after long-term high exposure—a study in Ronneby, Sweden. *Environment International* **163**, 107198.
- Li, Y., Fletcher, T., Mucs, D., Scott, K., Lindh, C. H., Tallving, P., and Jakobsson, K. (2018). Half-lives of PFOS, PFHxS and PFOA after end of exposure to contaminated drinking water. *Occupational and Environmental Medicine* **75**, 46–51.

- Marques, I., Kneib, T., and Klein, N. (2022). Mitigating spatial confounding by explicitly correlating Gaussian random fields. *Environmetrics* **33**, e2727.
- National Academies of Sciences, Engineering, and Medicine (2022). *Guidance on PFAS Exposure, Testing, and Clinical Follow-Up*. The National Academies Press, Washington, DC.
- Paciorek, C. J. (2010). The importance of scale for spatial-confounding bias and precision of spatial regression estimators. *Statistical Science* **25**, 107–125.
- R Core Team (2023). *R: A Language and Environment for Statistical Computing*. R Foundation for Statistical Computing, Vienna, Austria.
- Rasmussen, C. E. and Williams, C. K. I. (2005). *Gaussian Processes for Machine Learning*. The MIT Press.
- Reich, B. J., Hodges, J. S., and Zadnik, V. (2006). Effects of residual smoothing on the posterior of the fixed effects in disease-mapping models. *Biometrics* **62**, 1197–1206.
- Ribeiro Jr, P. J., Diggle, P., Christensen, O., Schlather, M., Bivand, R., and Ripley, B. (2023). *geoR: Analysis of Geostatistical Data*. R package version 1.9-3.
- Rice, J. (1986). Convergence rates for partially splined models. *Statistics & Probability Letters* **4**, 203–208.
- Robins, J. M., Li, L., Mukherjee, R., Tchetgen, E. T., and van der Vaart, A. (2017). Minimax estimation of a functional on a structured high-dimensional model. *The Annals of Statistics* **45**, 1951–1987.
- Robinson, P. M. (1988). Root-n-consistent semiparametric regression. *Econometrica* **56**, 931–954.
- Schlather, M., Malinowski, A., Menck, P. J., Oesting, M., and Stokorb, K. (2015). Analysis, simulation and prediction of multivariate random fields with package randomfields. *Journal of Statistical Software* **63**, 1–25.

- Schnell, P. M. and Papadogeorgou, G. (2020). Mitigating unobserved spatial confounding when estimating the effect of supermarket access on cardiovascular disease deaths. *The Annals of Applied Statistics* **14**, 2069 – 2095.
- Stein, M. (1999). *Interpolation of Spatial Data: Some Theory for Kriging*. Springer Series in Statistics. Springer New York.
- Sun, M., Arevalo, E., Strynar, M., Lindstrom, A., Richardson, M., Kearns, B., Pickett, A., Smith, C., and Knappe, D. R. (2016). Legacy and emerging perfluoroalkyl substances are important drinking water contaminants in the Cape Fear River Watershed of North Carolina. *Environmental Science & Technology Letters* **3**, 415–419.
- Thaden, H. and Kneib, T. (2018). Structural equation models for dealing with spatial confounding. *The American Statistician* **72**, 239–252.
- Vecchia, A. V. (1988). Estimation and model identification for continuous spatial processes. *Journal of the Royal Statistical Society. Series B (Methodological)* **50**, 297–312.
- Wallis, D. J., Kotlarz, N., Knappe, D. R., Collier, D. N., Lea, C. S., Reif, D., McCord, J., Strynar, M., DeWitt, J. C., and Hoppin, J. A. (2023). Estimation of the half-lives of recently detected per-and polyfluorinated alkyl ethers in an exposed community. *Environmental Science & Technology* **57**, 15348–15355.
- Weisskopf, M. G., Seals, R. M., and Webster, T. F. (2018). Bias amplification in epidemiologic analysis of exposure to mixtures. *Environmental Health Perspectives* **126**, 047003.
- Wood, S. N. (2011). Fast stable restricted maximum likelihood and marginal likelihood estimation of semiparametric generalized linear models. *Journal of the Royal Statistical Society: Series B (Statistical Methodology)* **73**, 3–36.
- Wood, S. N. (2017). *Generalized Additive Models: An Introduction With R, Second Edition*. CRC press.
- Zhang, Y., Beeson, S., Zhu, L., and Martin, J. W. (2013). Biomonitoring of perfluoroalkyl

acids in human urine and estimates of biological half-life. *Environmental Science & Technology* **47**, 10619–10627.

SUPPORTING INFORMATION

Web Appendices and Tables referenced in Sections 1, 2.2, 2.3, 3, 3.2, and 3.3 are available in the following supplemental sections. Code for DSR estimators and simulation studies is available on GitHub at <https://github.com/nbwiecha/Double-Spatial-Regression>.

S1. OVERVIEW OF RELATED SEMIPARAMETRIC THEORY

S1.1 *Overview of related semiparametric theory*

This section briefly summarizes the semiparametric literature on root- n consistency and asymptotic normality of estimators similar to gSEM. More complete explanations can be found in Andrews (1994) and Chernozhukov et al. (2018). For $i \in \{1, \dots, n\}$, let $Y_i \in \mathbb{R}$ be the response variable, A_i be the treatment variable, and \mathbf{S}_i be the spatial location contained in spatial domain $\mathcal{S} \subset \mathbb{R}^d$. A simple model is:

$$\begin{aligned} Y_i &= A_i \beta_0 + g_0(\mathbf{S}_i) + U_i \\ A_i &= m_0(\mathbf{S}_i) + V_i. \end{aligned} \tag{12}$$

For illustration in this section we ignore covariates and assume A_i is a scalar. In (12), β_0 is the regression coefficient of interest, g_0 and m_0 are unknown functions treated as nuisance parameters, and U_i and V_i are error terms with finite, non-zero variance such that $E(U_i|A_i, \mathbf{S}_i) = 0$ and $E(V_i|\mathbf{S}_i) = 0$ for $i = 1, \dots, n$. Denote by $h_0(\mathbf{s}) := E(Y_i|\mathbf{S}_i = \mathbf{s})$ (marginalizing over A_i), and let η_0 denote the vector of functions (g_0, m_0) or (h_0, m_0) .

Model (12) can result in invalid inference due to spatial confounding if g_0, m_0 result in dependence between \mathbf{A} and $g_0(\mathbf{S})$. For example, if $g_0 = m_0$, this corresponds to an unmeasured confounder which is a function of space affecting both Y_1, \dots, Y_n and A_1, \dots, A_n , and in a spatial linear mixed model, this dependence is typically ignored. For example, spatial

random effects are commonly used to implement a smoother to model the unknown function g_0 , but are usually marginalized into the conditional variance of \mathbf{Y} without consideration of dependence with \mathbf{A} (Paciorek, 2010). Alternatively, some basis functions used to model g_0 may be collinear with \mathbf{A} , in which case penalized estimation of the coefficients on the basis functions leads to bias in estimation of β_0 (Reich et al., 2006).

Algorithm S2 Geoaddivitive Structural Equation Model (gSEM) estimation of β_0

Input: Response vector $\mathbf{Y} \in \mathbb{R}^n$, location matrix $\mathbf{S} \in \mathbb{R}^{n \times d}$, treatment vector $\mathbf{A} \in \mathbb{R}^n$

Output: Estimate $\hat{\beta}_{gSEM}$ of $\beta_0 \in \mathbb{R}$

$\hat{h}_0 \leftarrow$ Estimate of h_0 from a spatial regression model for \mathbf{Y} onto \mathbf{S} , such as a spline regression

$\mathbf{R}_Y \leftarrow \mathbf{Y} - \hat{h}_0(\mathbf{S})$

$\hat{m}_0 \leftarrow$ Estimate of m_0 from a spatial regression model for \mathbf{A} onto \mathbf{S} , such as a spline regression

$\mathbf{R}_A \leftarrow \mathbf{A} - \hat{m}_0(\mathbf{S})$

$\hat{\beta}_{gSEM} \leftarrow (\mathbf{R}_A^T \mathbf{R}_A)^{-1} \mathbf{R}_A^T \mathbf{R}_Y$, i.e., obtain $\hat{\beta}_0$ by regressing the residuals \mathbf{R}_Y onto the residuals \mathbf{R}_A

Return $\hat{\beta}_{gSEM}$

The gSEM procedure is in Algorithm S2. Variance is typically estimated via bootstrap when gSEM is used in simulation studies (Guan et al., 2022; Gilbert et al., 2021). Aside from the method of estimating h_0 and m_0 and variance estimation, this is identical to the procedure considered in Robinson (1988). Intuitively, it is approximately orthogonalizing \mathbf{Y} and \mathbf{A} with respect to \mathbf{S} and therefore removing effects of spatial confounding.

S1.1.1 *Orthogonality of $\hat{\beta}_{gSEM}$ and nuisance parameter estimates.* To study $\hat{\beta}_{gSEM}$'s asymptotic properties, note that $\hat{\beta}_{gSEM}$ is equivalently defined as the solution to

$$\frac{1}{n} \sum_{i=1}^n \psi(Y_i, A_i, \mathbf{S}_i; \hat{\beta}_{gSEM}, \hat{\eta}_0) = 0$$

where $\psi(Y_i, A_i, \mathbf{S}_i; \beta, \eta) = \{Y_i - h(\mathbf{S}_i) - \beta(A_i - m(\mathbf{S}_i))\}(A_i - m(\mathbf{S}_i))$, $\eta = (h, m)$, $\hat{\eta}_0 = (\hat{h}_0, \hat{m}_0)$, and \hat{h}_0 and \hat{m}_0 are preliminary estimates of the nuisance parameters h_0 and m_0 . The score function ψ is used in Robinson (1988), and also studied in Andrews (1994) and Chernozhukov et al. (2018). This score function results in a form of orthogonality between $\hat{\beta}_{gSEM}$ and $\hat{\eta}_0$: under the model (12), replacement of η_0 by $\hat{\eta}_0$ in $\frac{1}{n} \sum_{i=1}^n E[\psi(Y_i, A_i, \mathbf{S}_i; \beta_0, \eta_0)]$ has an effect that is $o_P(n^{-1/2})$ when $\hat{\eta}_0$ is close to η_0 and \hat{h}_0, \hat{m}_0 each converge to their true values at $o_P(n^{-1/4})$ rate and obey smoothness conditions, and other regularity conditions are assumed (Andrews, 1994).¹ Alternatively, Chernozhukov et al. (2018) uses the term (near-) Neyman orthogonality. Neyman orthogonality means that the Gateaux functional derivative² with respect to η is 0 at the true nuisance parameter values:

$$\partial_\eta E[\psi(Y_i, A_i, \mathbf{S}_i; \beta_0, \eta_0)][\eta - \eta_0] = 0,$$

and in the case of near-Neyman orthogonality, that it is $o_P(n^{-1/2})$. Similarly, this indicates that close to η_0 , there is little effect on $E[\psi(Y_i, A_i, \mathbf{S}_i; \beta_0, \eta_0)]$ when replacing η_0 by its estimate. The orthogonality property means that the estimates \hat{h}_0 and \hat{m}_0 can converge to h_0 and m_0 at rates slower than $o_P(n^{-1/2})$ and asymptotically this deviation from (h_0, m_0) does not affect the variance of $\hat{\beta}_{gSEM}$ (Andrews, 1994).

S1.1.2 *Stochastic equicontinuity or sample splitting.* The orthogonality property of ψ must be paired with a means of ensuring that estimation error of η_0 does not cause asymptotic

¹Estimating the nuisance parameters using spline regression may not meet the sufficient conditions for good asymptotic behavior presented in (Andrews, 1994), which used nonparametric kernel regression estimators.

²Using the notation of Chernozhukov et al. (2018), the Gateaux derivative is defined as $D_r[\eta - \eta_0] := \partial_r \left\{ E[\psi(W; \beta_0, \eta_0 + r(\eta - \eta_0))] \right\}$ for $r \in [0, 1)$, $\eta \in T$ where T is a convex subspace of a normed vector space, and $\partial_\eta E[\psi(W; \beta_0, \eta_0)] := D_0[\eta - \eta_0]$.

bias, primarily due to overfitting (Chernozhukov et al., 2018). This is achieved by a property of empirical processes called stochastic equicontinuity in Andrews (1994) and by sample splitting in Chernozhukov et al. (2018). Stochastic equicontinuity follows from Donsker conditions (Belloni et al., 2017) which limit the complexity of η_0 and $\hat{\eta}_0$. In Andrews (1994), these are primarily satisfied by placing a smoothness requirement on η_0 and $\hat{\eta}_0$. In contrast, the sample-splitting approach of Chernozhukov et al. (2018) avoids requiring Donsker conditions, and therefore additional smoothness requirements. Since by using sample splitting Chernozhukov et al. (2018) allows estimation of η_0 by essentially any machine learning model, they term their method Double Machine Learning (DML). By using cross-fitting, the DML estimators of Chernozhukov et al. (2018) still use the full sample so do not lose power. We therefore rely on Chernozhukov et al. (2018) for our theoretical analysis of an estimator similar to gSEM, and term this estimator Double Spatial Regression since we are using Double Machine Learning with spatial regression.

S2. SMOOTHNESS CONDITIONS

To provide intuition on Assumption A6, the following explanation of Besov spaces is paraphrased from Eberts and Steinwart (2013). Denote the ζ -th weak derivative $\partial^{(\zeta)}$ for a multi-index $\zeta = (\zeta_1, \zeta_2, \dots, \zeta_d) \in \mathbb{N}^d$ with $|\zeta| = \sum_{i=1}^d \zeta_i$. With regard to a measure ν , the Sobolev space $W_p^\alpha(\nu)$ is defined as:

$$W_p^\alpha(\nu) := \{f \in L_p(\nu) : \partial^{(\zeta)} f \in L_p(\nu) \text{ exists for all } \zeta \in \mathbb{N}^d \text{ with } |\zeta| < \alpha\}.$$

Loosely speaking, $W_p^\alpha(\nu)$ is the space of functions with α weak derivatives, which all must have finite $L_p(\nu)$ norm. We refer to Eberts and Steinwart (2013) for a full definition of Besov spaces $B_{p,q}^\alpha$, but Besov spaces provide a finer scale of smoothness than the integer-ordered Sobolev spaces, and Sobolev spaces are contained in the Besov spaces:

$$W_p^\alpha(\mathbb{R}^d) \subset B_{p,q}^\alpha(\mathbb{R}^d)$$

for $\alpha \in \mathbb{N}, p \in (1, \infty), \max\{p, 2\} \leq q \leq \infty$.

A stronger, but more interpretable alternative to the assumption that $h_0 \in B_{2s, \infty}^{\alpha_Y}$ and $m_{01}, \dots, m_{0p} \in B_{2s, \infty}^{\alpha_X}$ in assumption A6 is that the m_{0j} reside in the integer-order Sobolev space $W_{2s}^{\alpha'_X}$ and h_0 resides in the integer-order Sobolev space $W_{2s}^{\alpha'_Y}$, where $\alpha'_X = [\alpha_X]$ and $\alpha'_Y = [\alpha_Y]$ and $[a]$ indicates the lowest integer greater than a . In the common scenario $d = 2$, the requirements on α_X and α_Y reduce to $\alpha_X > 1$ and $\alpha_Y > 1$, which for integer-ordered Sobolev spaces, loosely means that both h_0 and m_0 have at least two partial derivatives.

S3. ADDITIONAL ALGORITHMS

Below are the algorithms for the more practical DSR estimators. They use the following Kriging equations.

If cross-fitting is used, the equations on fold k are:

$$\hat{g}_0(\mathbf{S}_{\mathbf{k}}) = \hat{\omega}_{0k} C_{\hat{\gamma}_{0k}, \hat{\tau}_{0k}}(\mathbf{S}_{\mathbf{k}}, \mathbf{S}_{\mathbf{k}^c}) \left(\hat{\omega}_{0k} C_{\hat{\gamma}_{0k}, \hat{\tau}_{0k}}(\mathbf{S}_{\mathbf{k}^c}, \mathbf{S}_{\mathbf{k}^c}) + \hat{\sigma}_{0k}^2 \mathbf{I} \right)^{-1} \times (\mathbf{Y}_{\mathbf{k}^c} - \mathbf{A}_{\mathbf{k}^c}^T \hat{\boldsymbol{\beta}}_{0k} - \mathbf{Z}_{\mathbf{k}^c}^T \hat{\boldsymbol{\theta}}_{0k}) \quad (13)$$

$$\hat{m}_{0j}(\mathbf{S}_{\mathbf{k}}) = \hat{\omega}_{jk} C_{\hat{\gamma}_{jk}, \hat{\tau}_{jk}}(\mathbf{S}_{\mathbf{k}}, \mathbf{S}_{\mathbf{k}^c}) \left(\hat{\omega}_{jk} C_{\hat{\gamma}_{jk}, \hat{\tau}_{jk}}(\mathbf{S}_{\mathbf{k}^c}, \mathbf{S}_{\mathbf{k}^c}) + \hat{\sigma}_{0j}^2 \mathbf{I} \right)^{-1} (\mathbf{A}_{\mathbf{k}^c, j} - \mathbf{Z}_{\mathbf{k}^c}^T \hat{\boldsymbol{\theta}}_{jk}), \quad (14)$$

If cross-fitting is not used, the Universal Kriging equations are:

$$\hat{g}_0(\mathbf{S}) = \hat{\omega}_0^2 C_{\hat{\gamma}_0, \hat{\tau}_0}(\mathbf{S}, \mathbf{S}) \left(\hat{\omega}_0^2 C_{\hat{\gamma}_0, \hat{\tau}_0}(\mathbf{S}, \mathbf{S}) + \hat{\sigma}_0^2 \mathbf{I} \right)^{-1} (\mathbf{Y} - \mathbf{A}^T \tilde{\boldsymbol{\beta}}_0 - \mathbf{Z}^T \hat{\boldsymbol{\theta}}_0) \quad (15)$$

$$\hat{m}_{0j}(\mathbf{S}) = \hat{\omega}_j^2 C_{\hat{\gamma}_j, \hat{\tau}_j}(\mathbf{S}, \mathbf{S}) \left(\hat{\omega}_j^2 C_{\hat{\gamma}_j, \hat{\tau}_j}(\mathbf{S}, \mathbf{S}) + \hat{\sigma}_j^2 \mathbf{I} \right)^{-1} (\mathbf{A}_j - \mathbf{Z}^T \hat{\boldsymbol{\theta}}_j), \quad (16)$$

Algorithm S3 DSR estimation of β_0 with cross-fitting

Input: Response vector $\mathbf{Y} \in \mathbb{R}^n$, location matrix $\mathbf{S} \in \mathbb{R}^{n \times 2}$, treatment matrix $\mathbf{A} \in \mathbb{R}^{n \times \ell}$, covariate matrix $\mathbf{Z} \in \mathbb{R}^{n \times m}$.

Output: Estimate $\hat{\beta}_{DSR}$ of $\beta_0 \in \mathbb{R}^{\ell \times 1}$ and estimate $\widehat{Var}(\hat{\beta}_{DSR})$ of $Var(\hat{\beta}_{DSR}) \in \mathbb{R}^{\ell \times \ell}$

Partition the data into K random folds so that the size of each fold is $\frac{n}{K}$.

for $k = 1, \dots, K$ **do**

Obtain $\hat{\beta}_{0k}, \hat{\theta}_{0k}, \dots, \hat{\theta}_{\ell k}, \hat{\gamma}_{0k}, \dots, \hat{\gamma}_{\ell k}, \hat{\tau}_{0k}, \dots, \hat{\tau}_{\ell k}, \hat{\sigma}_{0k}, \dots, \hat{\sigma}_{\ell k}$ by REML using GpGp.

Obtain $\hat{g}_0(\mathbf{S}_{\mathbf{k}})$ by (8) (approximated by GpGp).

$\tilde{\mathbf{Y}}_{\mathbf{k}} \leftarrow \mathbf{Z}_{\mathbf{k}}^T \hat{\theta}_{0k} + \hat{g}_0(\mathbf{S}_{\mathbf{k}}); \tilde{\mathbf{Y}}_{\mathbf{k}} \in \mathbb{R}^{|\mathbf{k}|}$

for $j = 1, \dots, \ell$ **do**

Obtain $\hat{m}_{0j}(\mathbf{S}_{\mathbf{k}})$ by (9) (approximated by GpGp).

$\hat{\mathbf{A}}_{\mathbf{k},j} \leftarrow \mathbf{Z}_{\mathbf{k}}^T \hat{\theta}_{jk} + \hat{m}_{0j}(\mathbf{S}_{\mathbf{k}}); \hat{\mathbf{A}}_{\mathbf{k}} \in \mathbb{R}^{|\mathbf{k}|}$

end for

end for

Combine the estimates from each fold to obtain $\tilde{\mathbf{Y}} \in \mathbb{R}^n$, $\hat{\mathbf{A}} \in \mathbb{R}^{n \times \ell}$

$\hat{\mathbf{V}} \leftarrow \mathbf{A} - \hat{\mathbf{A}}$

$\hat{\mathbf{J}} \leftarrow (\hat{\mathbf{V}}^T \mathbf{A})^{-1}$

$\hat{\beta}_{DSR} \leftarrow \hat{\mathbf{J}} \hat{\mathbf{V}}^T (\mathbf{Y} - \tilde{\mathbf{Y}}); \hat{\beta}_{DSR} \in \mathbb{R}^{\ell}$

$\widehat{Var}(\hat{\beta}_{DSR}) \leftarrow \hat{\mathbf{J}} \left(\sum_{i=1}^n \left[-\hat{\mathbf{V}}_i \mathbf{A}_i^T \hat{\beta}_{DSR} + \hat{\mathbf{V}}_i (Y_i - \tilde{Y}_i) \right] \left[-\hat{\mathbf{V}}_i \mathbf{A}_i^T \hat{\beta}_{DSR} + \hat{\mathbf{V}}_i (Y_i - \tilde{Y}_i) \right]^T \right) \hat{\mathbf{J}}^T$

Return $\hat{\beta}_{DSR}, \widehat{Var}(\hat{\beta}_{DSR})$

Algorithm S4 DSR estimation of β_0 without cross-fitting

Input: Response vector $\mathbf{Y} \in \mathbb{R}^n$, location matrix $\mathbf{S} \in \mathbb{R}^{n \times 2}$, treatment matrix $\mathbf{A} \in \mathbb{R}^{n \times \ell}$, covariate matrix $\mathbf{Z} \in \mathbb{R}^{n \times m}$.

Output: Estimate $\hat{\beta}_{DSR}$ of $\beta_0 \in \mathbb{R}^{\ell \times 1}$ and estimate $\widehat{Var}(\hat{\beta}_{DSR})$ of $Var(\hat{\beta}_{DSR}) \in \mathbb{R}^{\ell \times \ell}$

Obtain $\hat{\beta}_0, \hat{\theta}_0, \dots, \hat{\theta}_\ell, \hat{\gamma}_0, \dots, \hat{\gamma}_\ell, \hat{\tau}_0, \dots, \hat{\tau}_\ell, \hat{\omega}_0^2, \dots, \hat{\omega}_\ell^2, \hat{\sigma}_0^2, \dots, \hat{\sigma}_\ell^2$ by REML using **GpGp**.

$\hat{g}(\mathbf{S})$ obtained by (15) (approximated by **GpGp**).

for $j = 1, \dots, \ell$ **do**

$\hat{m}_j(\mathbf{S})$ obtained by (16) (approximated by **GpGp**).

$\hat{\mathbf{A}}_j \leftarrow \mathbf{Z}^T \hat{\theta}_j + \hat{m}_j(\mathbf{S}); \hat{\mathbf{A}} \in \mathbb{R}^n$

end for

$\hat{\mathbf{V}} \leftarrow \mathbf{A} - \hat{\mathbf{A}}$

$\hat{\mathbf{J}} \leftarrow (\hat{\mathbf{V}}^T \mathbf{A})^{-1}$

$\hat{\beta}_{DSR} \leftarrow \hat{\mathbf{J}} \hat{\mathbf{V}}^T (\mathbf{Y} - \mathbf{Z}^T \hat{\theta}_0 - \hat{g}(\mathbf{S})); \hat{\beta}_{DSR} \in \mathbb{R}^\ell$

$\widehat{Var}(\hat{\beta}_{DSR}) \leftarrow \hat{\mathbf{J}} \left(\sum_{i=1}^n \left[\hat{\mathbf{V}}_i (Y_i - \mathbf{A}_i^T \hat{\beta}_{DSR} - \mathbf{Z}_i^T \hat{\theta}_0 - \hat{g}(\mathbf{S}_i)) \right] \left[\hat{\mathbf{V}}_i (Y_i - \mathbf{A}_i^T \hat{\beta}_{DSR} - \mathbf{Z}_i^T \hat{\theta}_0 - \hat{g}(\mathbf{S}_i)) \right]^T \right) \hat{\mathbf{J}}^T$

Return $\hat{\beta}_{DSR}, \widehat{Var}(\hat{\beta}_{DSR})$

S4. ADDITIONAL SIMULATION SCENARIOS

- (1) Cubed confounder: $Y_i \sim N(\beta A_i + U_i^3, \sigma_Y^2)$.
- (2) Gamma errors in \mathbf{Y} : $Y_i = \beta A_i + U_i + \phi_i, \phi_i = q[\Phi(\epsilon_i/\sqrt{3})]$, where q is the quantile function for the Gamma(1, $1/\sqrt{3}$) distribution and Φ is the standard normal CDF, and $\epsilon_i \sim N(0, \sigma_Y^2)$.
- (3) ‘‘East-west’’ heteroskedasticity: $Y_i = \beta A_i + U_i + S_{1i} \epsilon_i$, where S_{1i} is the first coordinate of \mathbf{S}_i and $\epsilon_i \sim N(0, \sigma_Y^2)$.
- (4) ‘‘Middle-out’’ heteroskedasticity: $Y_i = \beta A_i + \sqrt{\frac{\omega(S_{1i})}{3}} U_i + \sqrt{1 - \omega(S_{1i})} \epsilon_i$, where $\omega(S_{1i}) = \Phi\left(\frac{S_{1i} - 0.5}{0.1}\right)$ and $\epsilon_i \sim N(0, \sigma_Y^2)$.

The last three are borrowed from Huiying Mao and Reich (2023). Five further scenarios were considered.

- (1) Higher variance in \mathbf{A} : $\sigma_A^2 = 1$, causing less confounding bias.
- (2) Very rough processes: Σ_A and Σ_U were Matèrn correlation matrices with smoothness 0.5, making adjustment more challenging due to very rough sample paths.
- (3) Gridded spatial locations: Theory requires random spatial locations, but this illustrates the method with (very regular) fixed spatial locations.
- (4) Deterministic function of space, same for \mathbf{A} and \mathbf{U} : To avoid over-stating the effectiveness of DSR when the latent functions of space are generated and estimated using GPs, the data were generated using: $Y_i = \beta_0 A_i + g_0(\mathbf{s}_i) + \epsilon_{0i}$, and $A_i = m_0(\mathbf{s}_i) + \epsilon_{1i}$, where $g_0(\mathbf{s}_i) = m_0(\mathbf{s}_i) = \cos(10s_{i1}) \sin(10s_{i2})$, $\epsilon_{0i} \stackrel{i.i.d.}{\sim} N(0, 1^2)$, and $\epsilon_{1i} \stackrel{i.i.d.}{\sim} N(0, 0.1^2)$.
- (5) Deterministic function of space, different for \mathbf{A} and \mathbf{U} : Similar to the previous scenario, but now $g_0(\mathbf{s}_i) = m_0(\mathbf{s}_i) + \sin(10s_{i1}) \sin(10s_{i2})$ and m_0 is defined as in the previous scenario.

S5. FULL SIMULATION RESULTS

In the following tables, the following methods were compared:

- OLS: ordinary least squares regression.
- LMM: Spatial linear mixed model, estimated using `GpGp` (Guinness, 2018).
- Spline (GCV): spline model estimated using `mgcv` (Wood, 2011), with smoothing parameter selected by generalized cross-validation, to minimize out-of-sample prediction error.
- Spline (REML): spline model estimated using `mgcv`, smoothing parameter selected by restricted maximum likelihood (REML); Wood (2017) states that this might reduce bias when the parametric component is collinear with smooth term.
- Spatial+: the method of Dupont et al. (2022).

- gSEM: the point-referenced version of Thaden and Kneib (2018), described in Algorithm S2.
- Shift (BART): the shift estimand implemented in Gilbert et al. (2021), using Bayesian Additive Regression Trees (Chipman et al., 2010), or BART, to obtain the preliminary nonparametric estimates. BART estimates were obtained from the R package `dbarts` Dorie (2024). Results only presented in Table S13 due to inability to obtain estimates in other scenarios. Variance estimates not obtained due to relatively high expense of bootstrapping.
- DSR (theory): the alternative/theoretical DSR estimator described in Algorithm 1.
- DSR (theory, no crossfit): the alternative DSR estimator described in Algorithm 1 but without crossfitting.
- DSR: The DSR estimator with crossfitting described in Algorithm S3.
- DSR: (no crossfit): the DSR estimator without crossfitting described in Algorithm S4.
- DSR (spline, no crossfit): the DSR estimator without crossfitting described in Algorithm S4 but with splines used instead of GP regression.
- DSR (theory, spline, no crossfit): the alternative DSR estimator described in Algorithm 1 but without crossfitting, and with splines used instead of GP regression. This is equivalent to the implementation of gSEM used, except that it has a closed-form variance estimate.

The following metrics were used to compare the methods:

- Bias: average difference between estimates and β_0 over the Monte Carlo iterations. In all simulations $\beta_0 = 0.5$.
- Rel. Bias: relative bias, equal to bias divided by β_0 .
- MSE: mean squared error of estimates over the Monte Carlo iterations.
- 95% CI Length: length of 95% confidence interval.
- 95% CI CVG: coverage, i.e. proportion of Monte Carlo iterations in which the 95% confidence interval included β_0 .

- Power: Proportion of Monte Carlo iterations in which the 95% confidence interval did not include 0.

[Table 5 about here.]

[Table 6 about here.]

[Table 7 about here.]

[Table 8 about here.]

[Table 9 about here.]

[Table 10 about here.]

[Table 11 about here.]

[Table 12 about here.]

[Table 13 about here.]

[Table 14 about here.]

[Table 15 about here.]

[Table 16 about here.]

[Table 17 about here.]

S6. PROOF OF THEOREM 1

Theorem 1 follows from an extension of Theorem 4.1 from (Chernozhukov et al., 2018), and Theorems 3.3 and 3.6 from (Eberts and Steinwart, 2013). This section extends Theorem 4.1 from (Chernozhukov et al., 2018) to the case of a vector treatment variable, and then verifies that Assumptions A1-A6 satisfy the necessary conditions to apply these results.

S6.1 Proof of DML with partially linear model

In this section we extend Theorem 4.1 from (Chernozhukov et al., 2018), which analyzes the partially linear model with a scalar treatment, to a vector treatment. The extension essentially follows the proof of Theorem 4.1 from (Chernozhukov et al., 2018) with slight changes.

We use “DML2”, which is Definition 3.2 from Chernozhukov et al. (2018), where rather than aggregating K different estimates from K different folds, cross-fitting on the K folds is performed followed by estimation of β_0 using the combined cross-fitted estimates.

The assumed model is:

$$\mathbf{Y} = \mathbf{X}\beta + g_0(\mathbf{S}) + \mathbf{U} \quad (17)$$

$$\mathbf{X}_j = m_{0j}(\mathbf{S}) + \mathbf{V}_j$$

with notation and definitions as in the main paper. Nuisance parameters and estimates η are assumed to be in T , a convex subset of some normed vector space.

The “practical” DSR estimator uses the score function:

$$\psi(\mathbf{W}; \beta, \eta) := \{Y - g(\mathbf{S}) - \mathbf{X}^T \beta\}(\mathbf{X} - m(\mathbf{S})) \quad (18)$$

However, for theory, we focus on the score function:

$$\psi(\mathbf{W}; \beta, \eta) := \{Y - h(\mathbf{S}) - (\mathbf{X} - m(\mathbf{S}))^T \beta\}(\mathbf{X} - m(\mathbf{S})) \quad (19)$$

Assumption 1 consists of those of Assumption 4.1 from Chernozhukov et al. (2018) but expanded to encompass the case $p > 1$, the length of β_0 , and with some other slight changes for theoretical convenience. Let $\{\delta_n\}$ and $\{\Delta_n\}$ be sequences of positive constants converging to 0. Let c, C , and q be fixed strictly positive constants such that $q > 4$, and let $K \geq 2$ be a fixed integer. For any $\eta = (\ell_1, \ell_2, \dots, \ell_m)$ for any positive integer m such that ℓ_1, \dots, ℓ_m are functions mapping \mathcal{S} to \mathbb{R} , denote $\|\eta\|_{P,q} = \max_{1, \dots, m} \{\|\ell_1\|_{P,q}, \dots, \|\ell_m\|_{P,q}\}$.

ASSUMPTION 1 (Regularity Conditions for partially linear regression model): Let \mathcal{P} be the collection of probability laws P for $\mathbf{W} = (Y, \mathbf{X}, \mathbf{S})$ such that

- a) Model (17) holds,
- b) $\|V_1\|_{P,q}, \dots, \|V_p\|_{P,q} \leq C$ and $\|\beta_0\|_\infty \leq C$,
- c) The eigenvalues of the matrix $E[U^2\mathbf{V}\mathbf{V}^T]$ are greater than or equal to c^2 and the matrix $E[\mathbf{V}\mathbf{V}^T]$ has singular values at least c and no greater than C ,
- d) $\|E[U^2|\mathbf{S}]\|_{P,\infty} \leq C$ and $\|E[V_j^2|\mathbf{S}]\|_{P,\infty} \leq C$ for $j = 1, \dots, p$,
- e) Given a random subset I of $[n]$ of size n/K , the nuisance parameter estimator $\hat{\eta}_0 = \hat{\eta}_0((\mathbf{W}_i)_{i \in I^c})$ obey the following conditions for all $n/K \geq 1$: with P -probability no less than $1 - \Delta_n$,

$$\|\hat{\eta}_0 - \eta_0\|_{P,\infty} \leq C, \|\hat{\eta}_0 - \eta_0\|_{P,2} \leq \delta_n,$$

and for the score ψ in (19), where $\hat{\eta} = (\hat{\ell}_0, \hat{m}_{10}, \dots, \hat{m}_{p0})$,

$$\|\hat{m}_{j0} - m_{j0}\|_{P,2} \times (\|\hat{m}_{j0} - m_{j0}\|_{P,2} + \|\hat{\ell}_0 - \ell_0\|_{P,2}) \leq \delta_n n^{-1/2} \text{ for } j = 1, \dots, p.$$

The following lemma is Theorem 4.1 from Chernozhukov et al. (2018) but expanded to the case $p > 1$.

LEMMA 1 (DML inference in the partially linear regression model with $p > 1$): *Suppose that Assumption 1 holds. Then the DML2 estimator constructed in Definition 3.2 of Chernozhukov et al. (2018) using the score (19) obeys*

$$\Sigma^{-1/2} \sqrt{n}(\hat{\beta}_0 - \beta_0) \xrightarrow{D} N(\mathbf{0}, \mathbf{I}_p),$$

uniformly over $P \in \mathcal{P}$, where $\Sigma = [E(\mathbf{V}\mathbf{V}^T)]^{-1} E(U^2\mathbf{V}\mathbf{V}^T) [E(\mathbf{V}\mathbf{V}^T)]^{-1}$. The result continues to hold if Σ is replaced by $\hat{\Sigma}$ from Theorem 3.2 from Chernozhukov et al. (2018).

The proof for Lemma 1 follows the proof of Theorem 4.1 in Chernozhukov et al. (2018) closely, only needing to add steps to deal with the vector-valued ψ and matrix-valued ψ^a , and changing some assumptions slightly for convenience. The proof verifies Assumptions 3.1 and 3.2 from Chernozhukov et al. (2018), from which the conclusion of Lemma 1 follows from Theorems 3.1 and 3.2 from Chernozhukov et al. (2018).

Proof. [Proof of Lemma 1] Observe that the score (19) is linear in β :

$$\begin{aligned}\psi(\mathbf{W}; \beta, \eta) &= \{Y - \ell(\mathbf{S}) - (\mathbf{X} - \mathbf{m}(\mathbf{S}))^T \beta\}(\mathbf{X} - \mathbf{m}(\mathbf{S})) = \psi^a(\mathbf{W}; \eta)\beta + \psi^b(\mathbf{W}; \eta), \\ \psi^a(\mathbf{W}; \eta) &= -(\mathbf{X} - \mathbf{m}(\mathbf{S}))(\mathbf{X} - \mathbf{m}(\mathbf{S}))^T, \quad \psi^b(\mathbf{W}; \eta) = (Y - \ell(\mathbf{S}))(\mathbf{X} - \mathbf{m}(\mathbf{S}))\end{aligned}$$

Therefore, it is sufficient to verify Assumptions 3.1 and 3.2 from Chernozhukov et al. (2018).

Let \mathcal{T}_n be the set of all $\eta = (\ell, m_1, \dots, m_p)$ consisting of P -square-integrable functions ℓ, m_1, \dots, m_p such that

$$\begin{aligned}\|\hat{\eta}_0 - \eta_0\|_{P,q} &\leq C, \quad \|\hat{\eta}_0 - \eta_0\|_{P,2} \leq \delta_n, \\ \|\hat{m}_{j0} - m_{j0}\|_{P,2} \times (\|\hat{m}_{j0} - m_{j0}\|_{P,2} + \|\hat{\ell}_0 - \ell_0\|_{P,2}) &\leq \delta_n n^{-1/2}.\end{aligned}$$

We replace the constant q and the sequence $\{\delta_n\}$ in Assumptions 3.1 and 3.2 from Chernozhukov et al. (2018) by $q/2$ and $\{\delta'_n\}$, with $\delta'_n = (2p^2C + \sqrt{C}p + \sqrt{pC} + pC + pC\sqrt{pC} + \sqrt{pp}C^2 + 4\sqrt{p})(\delta_n \vee n^{-(1-4/q)\wedge(1/2)})$ for all n . As in Chernozhukov et al. (2018), we use five steps.

Step 1. Verify Neyman orthogonality. Note that $E[\psi(\mathbf{W}; \beta_0, \eta_0)] = 0$ by the definitions of β_0, η_0 . For any $\eta \in \mathcal{T}_n$, the Gateaux derivative in the direction $\eta - \eta_0$ is given by, for $r = 0$, (see derivation in Step 5):

$$\begin{aligned}\partial_\eta E[\psi(\mathbf{W}; \beta_0, \eta_0)][\eta - \eta_0] &= -E[(Y - \ell_0(\mathbf{S}))(\mathbf{m}(\mathbf{S}) - \mathbf{m}_0(\mathbf{S}))] - E[(\ell(\mathbf{S}) - \ell_0(\mathbf{S}))(\mathbf{D} - \mathbf{m}_0(\mathbf{S}))] \\ &\quad + E[(\mathbf{D} - \mathbf{m}_0(\mathbf{S}))(\mathbf{m}(\mathbf{S}) - \mathbf{m}_0(\mathbf{S}))^T \beta_0] \\ &\quad + E[(\mathbf{m}(\mathbf{S}) - \mathbf{m}_0(\mathbf{S}))(\mathbf{D} - \mathbf{m}_0(\mathbf{S}))^T \beta_0].\end{aligned}$$

By the law of iterated expectation, and since $\mathbf{V} = \mathbf{X} - \mathbf{m}_0(\mathbf{S})$ and $U = Y - \ell_0(\mathbf{S})$:

$$\begin{aligned}\partial_\eta E[\psi(\mathbf{W}; \beta_0, \eta_0)][\eta - \eta_0] &= E\{E[U \times (\mathbf{m}(\mathbf{S}) - \mathbf{m}_0(\mathbf{S})) | \mathbf{X}, \mathbf{S}]\} \\ &\quad - E\{E[(\ell(\mathbf{S}) - \ell_0(\mathbf{S}))\mathbf{V} | \mathbf{S}]\} \\ &\quad + E\{E[(\mathbf{m}(\mathbf{S}) - \mathbf{m}_0(\mathbf{S}))\mathbf{V}^T \beta_0 | \mathbf{S}]\} \\ &\quad + E\{E[\mathbf{V}(\mathbf{m}(\mathbf{S}) - \mathbf{m}_0(\mathbf{S}))^T \beta_0 | \mathbf{S}]\},\end{aligned}$$

which is equal to 0 since $E[\mathbf{V}|\mathbf{S}] = \mathbf{0}$ and $E[U|\mathbf{X}, \mathbf{S}] = 0$. This gives Assumption 3.1(d) from Chernozhukov et al. (2018) with $\lambda_n = 0$.

Step 2. By definition,

$$\begin{aligned} J_0 &= E[\psi^a(\mathbf{W}; \eta_0)] \\ &= E[-(\mathbf{X} - \mathbf{m}_0(\mathbf{S}))(\mathbf{X} - \mathbf{m}_0(\mathbf{S}))^T] \\ &= E[-\mathbf{V}\mathbf{V}^T] \end{aligned}$$

By assumption 1(c), the singular values of this matrix are between c_0 and C . This satisfies Assumption 3.1 (e) from Chernozhukov et al. (2018). Since the map $\eta \mapsto E[\psi(\mathbf{W}; \beta_0, \eta)]$ is twice Gateux-differentiable in T , this completes verification of Assumption 3.1 from Chernozhukov et al. (2018).

Step 3. Assumption 3.2(a) from Chernozhukov et al. (2018) holds by construction of \mathcal{T}_n and Assumption 1(e). In addition, $\psi(\mathbf{W}; \beta_0, \eta_0) = U\mathbf{V}$, so the eigenvalues of the matrix

$$E[\psi(\mathbf{W}; \beta_0, \eta_0)\psi(\mathbf{W}; \beta_0, \eta_0)^T] = E[U^2\mathbf{V}\mathbf{V}^T]$$

are bounded below by c_0 by Assumption 1(c). This verifies Assumption 3.2(d) from Chernozhukov et al. (2018).

Step 4. Next, we verify Assumption 3.2(b) from Chernozhukov et al. (2018). For any

$$\eta = (\ell, \mathbf{m}) \in \mathcal{T}_n,$$

$$\begin{aligned} m'_n &= E[\|\psi^a(\mathbf{S}; \eta)\|^{q/2}]^{2/q} \\ &= \left\| \|(\mathbf{X} - \mathbf{m}(\mathbf{S}))(\mathbf{X} - \mathbf{m}(\mathbf{S}))^T\| \right\|_{P,q/2} \\ &\leq \left\| \|(\mathbf{X} - \mathbf{m}_0(\mathbf{S}))(\mathbf{X} - \mathbf{m}_0(\mathbf{S}))^T\| + \|(\mathbf{X} - \mathbf{m}_0(\mathbf{S}))(\mathbf{m}_0(\mathbf{S}) - \mathbf{m}(\mathbf{S}))^T\| \right. \\ &\quad \left. + \|(\mathbf{m}_0(\mathbf{S}) - \mathbf{m}(\mathbf{S}))(\mathbf{X} - \mathbf{m}_0(\mathbf{S}))^T\| + \|(\mathbf{m}_0(\mathbf{S}) - \mathbf{m}(\mathbf{S}))(\mathbf{m}_0(\mathbf{S}) - \mathbf{m}(\mathbf{S}))^T\| \right\|_{P,q/2} \\ &= \left\| \|\mathbf{V}\mathbf{V}^T\| + 2\|\mathbf{V}(\mathbf{m}_0(\mathbf{S}) - \mathbf{m}(\mathbf{S}))^T\| + \|(\mathbf{m}_0(\mathbf{S}) - \mathbf{m}(\mathbf{S}))(\mathbf{m}_0(\mathbf{S}) - \mathbf{m}(\mathbf{S}))^T\| \right\|_{P,q/2} \\ &\leq \left\| \|\mathbf{V}\mathbf{V}^T\|_{P,q/2} + 2\|\|\mathbf{V}(\mathbf{m}_0(\mathbf{S}) - \mathbf{m}(\mathbf{S}))^T\|\|_{P,q/2} + \|\|(\mathbf{m}_0(\mathbf{S}) - \mathbf{m}(\mathbf{S}))(\mathbf{m}_0(\mathbf{S}) - \mathbf{m}(\mathbf{S}))^T\|\|_{P,q/2} \right\|_{P,q/2} \\ &= \left\| \|\mathbf{V}\|^2_{P,q/2} + 2\|\|\mathbf{V}\| \times \|(\mathbf{m}_0(\mathbf{S}) - \mathbf{m}(\mathbf{S}))\|\|_{P,q/2} + \|\|(\mathbf{m}_0(\mathbf{S}) - \mathbf{m}(\mathbf{S}))\|^2\|_{P,q/2} \right\|_{P,q/2} \\ &\leq \left\| \|\mathbf{V}\|^2_{P,q} + 2\|\|\mathbf{V}\|\|_{P,q} \times \|\|\mathbf{m}_0(\mathbf{S}) - \mathbf{m}(\mathbf{S})\|\|_{P,q} + \|\|\mathbf{m}_0(\mathbf{S}) - \mathbf{m}(\mathbf{S})\|^2\|_{P,q} \right\|_{P,q}, \end{aligned}$$

by the triangle inequality for the $\|\cdot\|$ -norm, the triangle inequality for the $\|\cdot\|_{P,q/2}$ -norm, the fact that for vectors \mathbf{u} and \mathbf{v} , $\|\mathbf{u}\mathbf{v}^T\| = \|\mathbf{u}\|\|\mathbf{v}\|$, and by the Cauchy-Schwarz inequality. Note that for a random vector \mathbf{Z} with p elements, if $\|Z_j\|_{P,q} < C$ for $j = 1, \dots, p$, then $\|\|\mathbf{Z}\|\|_{P,q} \leq \|\|\mathbf{Z}\|_1\|_{P,q} \leq \|Z_1\|_{P,q} + \dots + \|Z_p\|_{P,q} \leq pC$, by the fact that $\|\mathbf{Z}\| \leq \|\mathbf{Z}\|_1$ and monotonicity of expectation, then the triangle inequality, then the assumption that $\|Z_j\|_{P,q} < C$ for $j = 1, \dots, p$. By assumption $\|V_1\|_{P,q} + \dots + \|V_p\|_{P,q} \leq C$. Also, for $\eta \in \mathcal{T}_n$, $\|\eta_0 - \eta\|_{P,q} < C$. Therefore we have that:

$$\begin{aligned} m'_n &\leq \left\| \|\mathbf{V}\|^2_{P,q} + 2\|\|\mathbf{V}\|\|_{P,q} \times \|\|\mathbf{m}_0(\mathbf{S}) - \mathbf{m}(\mathbf{S})\|\|_{P,q} + \|\|\mathbf{m}_0(\mathbf{S}) - \mathbf{m}(\mathbf{S})\|^2\|_{P,q} \right\|_{P,q} \\ &\leq (pC)^2 + 2(pC)(pC) + (pC)^2 = 4p^2C^2 \end{aligned}$$

bounding m'_n as desired.

Next we address m_n . Note that by assumption, $\|\beta_0\| < \sqrt{p}C$ since $\|\beta_0\|_\infty < C$. Note also

that $Y - \ell_0(\mathbf{S}) = U + \mathbf{V}^T \boldsymbol{\beta}_0$.

$$\begin{aligned}
m_n &= (E[\|\psi(\mathbf{W}; \boldsymbol{\beta}_0, \eta)\|^{q/2}])^{2/q} \\
&= \|\|\psi(\mathbf{W}; \boldsymbol{\beta}_0, \eta)\|_{P,q/2}\| \\
&= \|\|U\mathbf{V} + U(\mathbf{m}_0(\mathbf{S}) - \mathbf{m}(\mathbf{S})) + (\ell_0(\mathbf{S}) - \ell(\mathbf{S}))\mathbf{V} \\
&\quad + (\ell_0(\mathbf{S}) - \ell(\mathbf{S}))(\mathbf{m}_0(\mathbf{S}) - \mathbf{m}(\mathbf{S})) \\
&\quad - (\mathbf{m}_0(\mathbf{S}) - \mathbf{m}(\mathbf{S}))^T \boldsymbol{\beta}_0 \mathbf{V} - (\mathbf{m}_0(\mathbf{S}) - \mathbf{m}(\mathbf{S}))(\mathbf{m}_0(\mathbf{S}) - \mathbf{m}(\mathbf{S}))^T \boldsymbol{\beta}_0\|_{P,q/2} \\
&\leq \|\|U\mathbf{V}\| + \|U(\mathbf{m}_0(\mathbf{S}) - \mathbf{m}(\mathbf{S}))\| + \|(\ell_0(\mathbf{S}) - \ell(\mathbf{S}))\mathbf{V}\| + \|(\ell_0(\mathbf{S}) - \ell(\mathbf{S}))(\mathbf{m}_0(\mathbf{S}) - \mathbf{m}(\mathbf{S}))\| \\
&\quad + \|(\mathbf{m}_0(\mathbf{S}) - \mathbf{m}(\mathbf{S}))^T \boldsymbol{\beta}_0 \mathbf{V}\| + \|(\mathbf{m}_0(\mathbf{S}) - \mathbf{m}(\mathbf{S}))(\mathbf{m}_0(\mathbf{S}) - \mathbf{m}(\mathbf{S}))^T \boldsymbol{\beta}_0\|_{P,q/2} \\
&\leq \|\|U\mathbf{V}\|_{P,q/2} + \|U(\mathbf{m}_0(\mathbf{S}) - \mathbf{m}(\mathbf{S}))\|_{P,q/2} + \|(\ell_0(\mathbf{S}) - \ell(\mathbf{S}))\mathbf{V}\|_{P,q/2} \\
&\quad + \|(\ell_0(\mathbf{S}) - \ell(\mathbf{S}))(\mathbf{m}_0(\mathbf{S}) - \mathbf{m}(\mathbf{S}))\|_{P,q/2} \\
&\quad + \|\|\mathbf{V}(\mathbf{m}_0(\mathbf{S}) - \mathbf{m}(\mathbf{S}))^T \boldsymbol{\beta}_0\|_{P,q/2} + \|(\mathbf{m}_0(\mathbf{S}) - \mathbf{m}(\mathbf{S}))(\mathbf{m}_0(\mathbf{S}) - \mathbf{m}(\mathbf{S}))^T \boldsymbol{\beta}_0\|_{P,q/2} \\
&\leq \|U\|_{P,q} \|\mathbf{V}\|_{P,q} + \|U\|_{P,q} \|\mathbf{m}_0(\mathbf{S}) - \mathbf{m}(\mathbf{S})\|_{P,q} + \|\ell_0(\mathbf{S}) - \ell(\mathbf{S})\|_{P,q} \|\mathbf{V}\|_{P,q} \\
&\quad + \|\ell_0(\mathbf{S}) - \ell(\mathbf{S})\|_{P,q} \|\mathbf{m}_0(\mathbf{S}) - \mathbf{m}(\mathbf{S})\|_{P,q} \\
&\quad + \|\|\mathbf{V}\|_{P,q} \|\mathbf{m}_0(\mathbf{S}) - \mathbf{m}(\mathbf{S})\|_{P,q} \|\boldsymbol{\beta}_0\| + \|\|\mathbf{m}_0(\mathbf{S}) - \mathbf{m}(\mathbf{S})\|_{P,q}^2 \|\boldsymbol{\beta}_0\| \\
&\leq pC^2 + pC^2 + pC^2 + pC^2 + p^2C^3 + p^2C^3 \\
&= 4pC^2 + 2p^2C^3,
\end{aligned}$$

bounding m_n as desired. The first two inequalities are due to the triangle inequality; the third inequality due to Cauchy-Schwartz; and the final inequality by assumed bounds on the quantities in the previous step and the bounds established in the derivation of the bound on m'_n above.

Step 5. Finally, we verify the conditions of Assumption 3.2(c) from Chernozhukov et al. (2018). Starting with $r_n = \sup_{\eta \in \mathcal{T}_n} \|E[\psi^a(\mathbf{W}; \eta)] - E[\psi^a(\mathbf{W}; \eta_0)]\|$,

$$\begin{aligned}
\|E[\psi^a(\mathbf{W}; \eta)] - E[\psi^a(\mathbf{W}; \eta_0)]\| &= \|E[\psi^a(\mathbf{W}; \eta) - \psi^a(\mathbf{W}; \eta_0)]\| \\
&= \|E[-(\mathbf{X} - \mathbf{m}(S))(\mathbf{X} - \mathbf{m}(S))^T + \mathbf{V}\mathbf{V}^T]\| \\
&\leq \|E[\mathbf{V}(\mathbf{m}_0(\mathbf{S}) - \mathbf{m}(\mathbf{S}))^T]\| + \|E[(\mathbf{m}_0(\mathbf{S}) - \mathbf{m}(\mathbf{S}))\mathbf{V}^T]\| \\
&\quad + \|E[(\mathbf{m}_0(\mathbf{S}) - \mathbf{m}(\mathbf{S}))(\mathbf{m}_0(\mathbf{S}) - \mathbf{m}(\mathbf{S}))^T]\| \\
&\leq 2E[\|\mathbf{V}\| \cdot \|(\mathbf{m}_0(\mathbf{S}) - \mathbf{m}(\mathbf{S}))\|] + E[\|(\mathbf{m}_0(\mathbf{S}) - \mathbf{m}(\mathbf{S}))\|^2] \\
&\leq 2\sqrt{E[\|\mathbf{V}\|^2]E[\|\mathbf{m}_0(\mathbf{S}) - \mathbf{m}(\mathbf{S})\|^2]} + E[\|\mathbf{m}_0(\mathbf{S}) - \mathbf{m}(\mathbf{S})\|^2] \\
&= 2\|\mathbf{V}\|_{P,2} \cdot \|\mathbf{m}_0(\mathbf{S}) - \mathbf{m}(\mathbf{S})\|_{P,2} + \|\mathbf{m}_0(\mathbf{S}) - \mathbf{m}(\mathbf{S})\|_{P,2}^2 \\
&\leq (pC)(p\delta_n) + (p^2C\delta_n) \\
&\leq \delta'_n
\end{aligned}$$

Where the first inequality is by the triangle inequality, the second inequality is by Jensen's inequality, the third inequality is by Cauchy-Schwarz, and the following inequality by the assumption that $\|V_j\|_{P,2} < C$ and $\|m_{0j} - m_j\|_{P,2} \leq \delta_n$ and $\|m_{0j} - m_j\|_{P,q} \leq C$ for $\eta \in \mathcal{T}_n$ for $j = 1, \dots, p$ and $q > 4$ (since $\|f\|_{P,q_1} \leq \|f\|_{P,q_2}$ for $0 < q_1 < q_2 < \infty$ by Jensen's inequality with $\phi(x) = |x|^{q_2/q_1}$). This establishes the bound on r_n .

Next we establish the bound on $r'_n = \sup_{\eta \in \mathcal{T}_n} (E[\|\psi(\mathbf{W}; \boldsymbol{\beta}_0, \eta) - \psi(\mathbf{W}; \boldsymbol{\beta}_0, \eta_0)\|^2])^{1/2}$:

$$\begin{aligned}
(E[\|\psi(\mathbf{W}; \boldsymbol{\beta}_0, \eta) - \psi(\mathbf{W}; \boldsymbol{\beta}_0, \eta_0)\|^2])^{1/2} &= \|\psi(\mathbf{W}; \boldsymbol{\beta}_0, \eta) - \psi(\mathbf{W}; \boldsymbol{\beta}_0, \eta_0)\|_{P,2} \\
&= \|\{Y - \ell(\mathbf{S}) - (\mathbf{X} - \mathbf{m}(\mathbf{S}))^T \boldsymbol{\beta}_0\}(\mathbf{X} - \mathbf{m}(\mathbf{S})) - \\
&\quad \{Y - \ell_0(\mathbf{S}) - (\mathbf{X} - \mathbf{m}_0(\mathbf{S}))^T \boldsymbol{\beta}_0\}(\mathbf{X} - \mathbf{m}_0(\mathbf{S}))\}\|_{P,2} \\
&\leq \|\|U(\mathbf{m}_0(\mathbf{S}) - \mathbf{m}(\mathbf{S}))\| + \|(\ell_0(\mathbf{S}) - \ell(\mathbf{S}))\mathbf{V}\| \\
&\quad + \|(\ell_0(\mathbf{S}) - \ell(\mathbf{S}))(\mathbf{m}_0(\mathbf{S}) - \mathbf{m}(\mathbf{S}))\| \\
&\quad + \|\mathbf{V}(\mathbf{m}_0(\mathbf{S}) - \mathbf{m}(\mathbf{S}))^T \boldsymbol{\beta}_0\| \\
&\quad + \|(\mathbf{m}_0(\mathbf{S}) - \mathbf{m}(\mathbf{S}))(\mathbf{m}_0(\mathbf{S}) - \mathbf{m}(\mathbf{S}))^T \boldsymbol{\beta}_0\|\|_{P,2} \\
&\leq \|\|U\| \cdot \|(\mathbf{m}_0(\mathbf{S}) - \mathbf{m}(\mathbf{S}))\|\|_{P,2} + \|\|\ell_0(\mathbf{S}) - \ell(\mathbf{S})\| \cdot \|\mathbf{V}\|\|_{P,2} \\
&\quad + \|\|\ell_0(\mathbf{S}) - \ell(\mathbf{S})\| \cdot \|(\mathbf{m}_0(\mathbf{S}) - \mathbf{m}(\mathbf{S}))\|\|_{P,2} \\
&\quad + \|\|\mathbf{V}(\mathbf{m}_0(\mathbf{S}) - \mathbf{m}(\mathbf{S}))^T \boldsymbol{\beta}_0\|\|_{P,2} \\
&\quad + \|\|(\mathbf{m}_0(\mathbf{S}) - \mathbf{m}(\mathbf{S}))(\mathbf{m}_0(\mathbf{S}) - \mathbf{m}(\mathbf{S}))^T \boldsymbol{\beta}_0\|\|_{P,2} \\
&\leq \|\|U\| \cdot \|(\mathbf{m}_0(\mathbf{S}) - \mathbf{m}(\mathbf{S}))\|\|_{P,2} + \|\|\ell_0(\mathbf{S}) - \ell(\mathbf{S})\| \cdot \|\mathbf{V}\|\|_{P,2} \\
&\quad + \|\|\ell_0(\mathbf{S}) - \ell(\mathbf{S})\| \cdot \|(\mathbf{m}_0(\mathbf{S}) - \mathbf{m}(\mathbf{S}))\|\|_{P,2} \\
&\quad + \|\|\mathbf{V}\| \cdot \|\mathbf{m}_0(\mathbf{S}) - \mathbf{m}(\mathbf{S})\|\|_{P,2} \|\boldsymbol{\beta}_0\| \\
&\quad + \|\|\mathbf{m}_0(\mathbf{S}) - \mathbf{m}(\mathbf{S})\|^2\|_{P,2} \|\boldsymbol{\beta}_0\| \\
&\leq \sqrt{C} p \delta_n + \sqrt{pC} \delta_n + pC \delta_n + \sqrt{pC} p \delta_n C + \sqrt{p} C p \delta_n C \\
&= (\sqrt{C} p + \sqrt{pC} + pC + \sqrt{pC} p C + \sqrt{p} C^2 p) \delta_n \\
&\leq \delta'_n
\end{aligned}$$

as desired, where the final inequality is due to the assumptions that $\|E[U^2|\mathbf{S}]\|_{P,\infty} \leq C$, $\|E[V_j^2|\mathbf{S}]\|_{P,\infty} \leq C$ for $j = 1, \dots, p$, and $\|\eta_0 - \eta\|_{P,\infty} \leq C$ for $\eta \in \mathcal{T}_n$, and applying the law of iterated expectation.

Finally we check the condition that $\lambda'_n = \sup_{r \in (0,1), \eta \in \mathcal{T}_n} \|\partial_r^2 E[\psi(\mathbf{W}; \boldsymbol{\beta}_0, \eta_0 + r(\eta - \eta_0))]\| \leq$

δ'_n/\sqrt{n} . Define $f(r) := E[\psi(\mathbf{W}; \boldsymbol{\beta}_0, \eta_0 + r(\eta - \eta_0)]$, $r \in (0, 1)$. Then for $r \in (0, 1)$,

$$\begin{aligned} \delta_r^2 f(r) &= E[2(\ell(\mathbf{S}) - \ell_0(\mathbf{S})) \times (\mathbf{m}(\mathbf{S}) - \mathbf{m}_0(\mathbf{S})) - 2(\mathbf{m}(\mathbf{S}) - \mathbf{m}_0(\mathbf{S}))(\mathbf{m}(\mathbf{S}) - \mathbf{m}_0(\mathbf{S}))^T \boldsymbol{\beta}_0] \\ &= 2E[(\ell(\mathbf{S}) - \ell_0(\mathbf{S})) \times (\mathbf{m}(\mathbf{S}) - \mathbf{m}_0(\mathbf{S}))] - 2E[(\mathbf{m}(\mathbf{S}) - \mathbf{m}_0(\mathbf{S}))(\mathbf{m}(\mathbf{S}) - \mathbf{m}_0(\mathbf{S}))^T \boldsymbol{\beta}_0] \end{aligned}$$

Then note that:

$$\begin{aligned} \|E[(\ell(\mathbf{S}) - \ell_0(\mathbf{S})) \times (\mathbf{m}(\mathbf{S}) - \mathbf{m}_0(\mathbf{S}))]\| &= \sqrt{\sum_{j=1}^p E[(\ell(\mathbf{S}) - \ell_0(\mathbf{S})) \times (m_j(\mathbf{S}) - m_{0j}(\mathbf{S}))]^2} \\ &\leq \sqrt{\sum_{j=1}^p E[(\ell(\mathbf{S}) - \ell_0(\mathbf{S}))^2] \times E[(m_j(\mathbf{S}) - m_{0j}(\mathbf{S}))^2]} \\ &= \sqrt{\sum_{j=1}^p \|\ell - \ell_0\|_{P,2}^2 \times \|m_j - m_{0j}\|_{P,2}^2} \end{aligned}$$

For $\eta \in T$, $\|\ell - \ell_0\|_{P,2}^2 \times \|m_j - m_{0j}\|_{P,2}^2 \leq \delta_n^2 n^{-1}$, so:

$$\begin{aligned} \|E[(\ell(\mathbf{S}) - \ell_0(\mathbf{S})) \times (\mathbf{m}(\mathbf{S}) - \mathbf{m}_0(\mathbf{S}))]\| &\leq \sqrt{\sum_{j=1}^p \delta_n^2 n^{-1}} \\ &= \sqrt{p \delta_n^2 n^{-1}} \\ &= \sqrt{p} \delta_n n^{-1/2} \end{aligned}$$

By the same reasoning, $\|E[(\mathbf{m}(\mathbf{S}) - \mathbf{m}_0(\mathbf{S}))^2]\| \leq \sqrt{p} \delta_n n^{-1/2}$. Then, we have that $\|\partial_r^2 E[\psi(\mathbf{W}; \boldsymbol{\beta}_0, \eta_0 + r(\eta - \eta_0))]\| = \|2E[(\ell(\mathbf{S}) - \ell_0(\mathbf{S})) \times (\mathbf{m}(\mathbf{S}) - \mathbf{m}_0(\mathbf{S}))] - 2E[(\mathbf{m}(\mathbf{S}) - \mathbf{m}_0(\mathbf{S}))(\mathbf{m}(\mathbf{S}) - \mathbf{m}_0(\mathbf{S}))^T \boldsymbol{\beta}_0]\| \leq 2\|E[(\ell(\mathbf{S}) - \ell_0(\mathbf{S})) \times (\mathbf{m}(\mathbf{S}) - \mathbf{m}_0(\mathbf{S}))]\| + 2\|E[(\mathbf{m}(\mathbf{S}) - \mathbf{m}_0(\mathbf{S}))(\mathbf{m}(\mathbf{S}) - \mathbf{m}_0(\mathbf{S}))^T \boldsymbol{\beta}_0]\|$, which does not depend on r , so that for $\eta \in T$, $\|\partial_r^2 E[\psi(\mathbf{W}; \boldsymbol{\beta}_0, \eta_0 + r(\eta - \eta_0))]\| \leq 4\sqrt{p} \delta_n n^{-1/2} \leq \delta'_n n^{-1/2}$, establishing the desired bound on λ'_n .

With the conditions of Assumptions 3.1 and 3.2 from Chernozhukov et al. (2018) verified, Lemma 1 follows from Facts 3.1 and 3.2 from Chernozhukov et al. (2018).

Lemma 2 follows directly from Theorem 3.3 from (Eberts and Steinwart, 2013), using $\rho = \ln(n)$. Note that the estimated function from the least-squares SVM with Gaussian kernel and least-squares loss analyzed in (Eberts and Steinwart, 2013) is identical to the posterior mean of a Gaussian process with Gaussian kernel; see e.g. (Kanagawa et al., 2018).

LEMMA 2 (Convergence rate for bounded regression using GP posterior mean): *Let \hat{f} be an estimate of $f(S) = E(Y|S)$ obtained by a Gaussian process posterior mean, with Gaussian kernel, using parameters γ_n, λ_n selected by the training-validation scheme in (Eberts and Steinwart, 2013) using grids as specified in Algorithm 1. Let P_S be the marginal distribution of S over \mathbb{R}^d with support in the $\|\cdot\|_2$ -unit ball. Let the density of P_S be $p_S \in L_q(\mathbb{R}^d)$ for some $q \geq 1$, and let $f \in L_2(\mathbb{R}^d) \cap L_\infty(\mathbb{R}^d)$ and $f \in B_{2s,\infty}^\alpha$ for $\alpha \geq 1$ and $s \geq 1$ such that $\frac{1}{q} + \frac{1}{s} = 1$. Let $Y \in [-M, M], M > 0$ and let \hat{f} be clipped at $-M, M$.*

Then with probability no less than $1 - \frac{1}{n}$, $\|\hat{f} - f\|_{P,2} \leq C \log(n) n^{-\frac{\alpha}{2\alpha+d} + \xi}$, for all $\xi > 0$ and some $C > 0$.

Lemma 3 follows directly from Theorem 3.6 from (Eberts and Steinwart, 2013), using $\hat{\rho} = \ln(n)$ and $\bar{\rho} = \ln(n)$ and clipping the absolute value of the fitted function at $\min\{1, M_n\}$ rather than simply M_n , which does not change the result since by assumption the true function lies in $[-1, 1]$. Note that per the proof of Theorem 3.6, the constant C in the original statement of Theorem 3.6 does not depend on either $\hat{\rho}$ or $\bar{\rho}$ allowing these substitutions.

LEMMA 3 (Convergence rate for regression with normal errors using GP posterior mean): *Let \hat{f} be an estimate of $f(S) = E(Y|S)$ obtained by a Gaussian process posterior mean, with Gaussian kernel, using parameters γ_n, λ_n selected by the training-validation scheme in (Eberts and Steinwart, 2013) using grids as specified in Algorithm 1. Let P_S be the marginal distribution of S over \mathbb{R}^d with support in the $\|\cdot\|_2$ -unit ball. Let the density of P_S be $p_S \in L_q(\mathbb{R}^d)$ for some $q \geq 1$, and let $f \in L_2(\mathbb{R}^d) \cap L_\infty(\mathbb{R}^d)$ and $f \in B_{2s,\infty}^\alpha$ for $\alpha \geq 1$ and $s \geq 1$ such that $\frac{1}{q} + \frac{1}{s} = 1$. Assume further that $f(S) \in [-1, 1]$.*

Let $Y_i = f(S_i) + \epsilon_i$ where $\epsilon_i \sim \text{ind. } N(0, \sigma_i^2)$, and let there exist some constant C_0 such that all $\sigma_i^2 < C_0$. Let \hat{f} be clipped so that $|\hat{f}| \leq \min\{1, M_n\}$ where $M_n = 4\sqrt{C_0}\sqrt{\ln(n)}$.

Then with probability no less than $1 - \frac{2}{n}$, $\|\hat{f} - f\|_{P,2} \leq C \log(n) n^{-\frac{\alpha}{2\alpha+2} + \xi}$, for all $\xi > 0$ and some $C > 0$.

The proof of Theorem 1 follows by verifying the Assumption 1 using assumptions A1-A6 and Facts 1-3.

Proof. [Proof of Theorem 1] First note that estimation of β_0 by $\hat{\beta}_{DSR}$ using Algorithm 1 is equivalent to using DML2 in Definition 3.2 of Chernozhukov et al. (2018), under the Partially Linear Regression DML estimation established by Lemma 1, and estimation of the nuisance parameters uses the same Gaussian Process (GP) estimates used in Facts 2 and 3. Therefore, the result of Theorem 1 follows from satisfying Assumption 1, which in turn is achieved in part by satisfying the assumptions for Facts 2 and 3 which establish the necessary convergence rates for prediction using GP regression.

In Assumption 1, (a) follows by Assumption A1, (b) follows from the assumption of bounded or normal distributions of U, V_j , so that all moments are finite, and the assumption that $\beta_0 \in \mathbb{R}^p$, and (c) and (d) follow from Assumption A2.

To satisfy (e) in Assumption 1, first note that by Assumption A4 the components of η_0 are bounded in some interval, and that the nuisance parameter estimates are clipped accordingly to reside in some interval, satisfying $\|\eta_0 - \hat{\eta}_0\|_{P,\infty} < C$ for some $C > 0$ (recall the notation $\|\eta_0 - \hat{\eta}_0\|_{P,q} = \max_j \|\eta_{0j} - \hat{\eta}_{0j}\|_{P,q}$ for $q \in [0, \infty)$). Next apply Lemmas 2 and 3 to satisfy the convergence rate requirements. Let $\alpha_X \geq \frac{d}{2}$ and $\alpha_X > 1$ per Assumption A6. Then if each m_{j0} is estimated by \hat{m}_{j0} using a Gaussian process mean with clipping at appropriate bounds as in Facts 2 and 3, then with probability no less than $1 - \frac{2}{n}$, $\|\hat{m}_{j0} - m_{j0}\|_{P,2} \leq C_j \log(n) n^{-\frac{\alpha_X}{2\alpha_X+d} + \xi}$ for any $\xi > 0$ and some $C_j > 0$, and $n^{-\frac{\alpha_X}{2\alpha_X+d}} < n^{-1/4}$. Let $\gamma = \frac{\alpha_X}{2\alpha_X+d} - 1/4 > 0$. Then with probability no less than $1 - \frac{2}{n}$, $\|\hat{m}_{j0} - m_{j0}\|_{P,2} \leq C_j \log(n) n^{-1/4} n^{-\gamma} n^\xi$, for all $\xi > 0$. Pick $\xi < \gamma$. Let $\gamma^* = \gamma - \xi > 0$. This holds for $j = 1, \dots, p$; let C_m be greater than or equal to all C_j . Then letting $\delta'_n = C_m (\log(n) n^{-\gamma^*}) \vee n^{-1/4} \rightarrow 0$, we have that $\|\hat{m}_{j0} - m_{j0}\|_{P,2} \leq \delta'_n n^{-1/4}$ with probability no less than $1 - \frac{2}{n}$ for all m_{0j} , $j = 1, \dots, p$, and if $\alpha_Y \geq \frac{d}{2}$ and $\alpha_Y > \frac{d^2}{4\alpha_X}$, the analogous result holds for g_0 as well.

Since all of the errors (of estimates of $g_0, m_{01}, \dots, m_{0p}$) individually obey the desired rates, each with marginal probability no less than $1 - \frac{\Delta}{n}$, there exists a sequence $\Delta \rightarrow 0$ such that with probability no less than $1 - \Delta_n$, all estimates of $g_0, m_{01}, \dots, m_{0p}$ simultaneously obey the desired error bounds. To see why, let $A_{kn}, k = 1, \dots, K, n = 1, 2, \dots$ be a finite number K of sequences of events, such that $P(A_{kn}) \rightarrow 1$ as $n \rightarrow \infty$ for each k . $P(A_{1n} \cup A_{2n}) = P(A_{1n}) + P(A_{2n}) - P(A_{1n} \cap A_{2n})$, and since $P(A_{1n} \cup A_{2n}) \geq P(A_{1n}), P(A_{2n})$, we have that $P(A_{1n} \cup A_{2n}) \rightarrow 1$ as $n \rightarrow \infty$. Hence, $\lim_{n \rightarrow \infty} P(A_{1n} \cap A_{2n}) = \lim_{n \rightarrow \infty} P(A_{1n}) + \lim_{n \rightarrow \infty} P(A_{2n}) - \lim_{n \rightarrow \infty} P(A_{1n} \cup A_{2n}) = 1$. Applying induction establishes that $\lim_{n \rightarrow \infty} P(A_{1n} \cap A_{2n} \cap \dots \cap A_{Kn}) = 1$. Therefore, there exists some sequence $L_n \rightarrow 0$ such that $P(A_{1n} \cap A_{2n} \cap \dots \cap A_{Kn}) \geq 1 - L_n$.

Therefore, there exists some sequence $\Delta_n \rightarrow 0$ such that $\|\hat{g}_0 - g_0\|_{P,2} \times \|\hat{m}_{0j} - m_{0j}\|_{P,2} \leq C\delta_n n^{-\frac{1}{2}}, \|\hat{m}_{0j} - m_{0j}\|_{P,2}^2 \leq C\delta_n n^{-\frac{1}{2}}$, and $\|\hat{\eta}_0 - \eta_0\|_{P,2} \leq \delta_n$ for $j = 1, \dots, p$, with $\delta_n = \delta_n'^2 \geq n^{-1/2}$, with probability no less than $1 - \Delta_n$.

Thus part (e) of Assumption 1 is satisfied.

With parts (a)-(e) of Assumption 1 satisfied, apply Lemma 1 to obtain $\widehat{Var}(\hat{\beta}_0)^{-1/2}(\hat{\beta}_0 - \beta_0) \xrightarrow{D} N(\mathbf{0}, \mathbf{I}_p)$.

Received July 2024. Revised XXXX 20XX. Accepted XXXX 20XX.

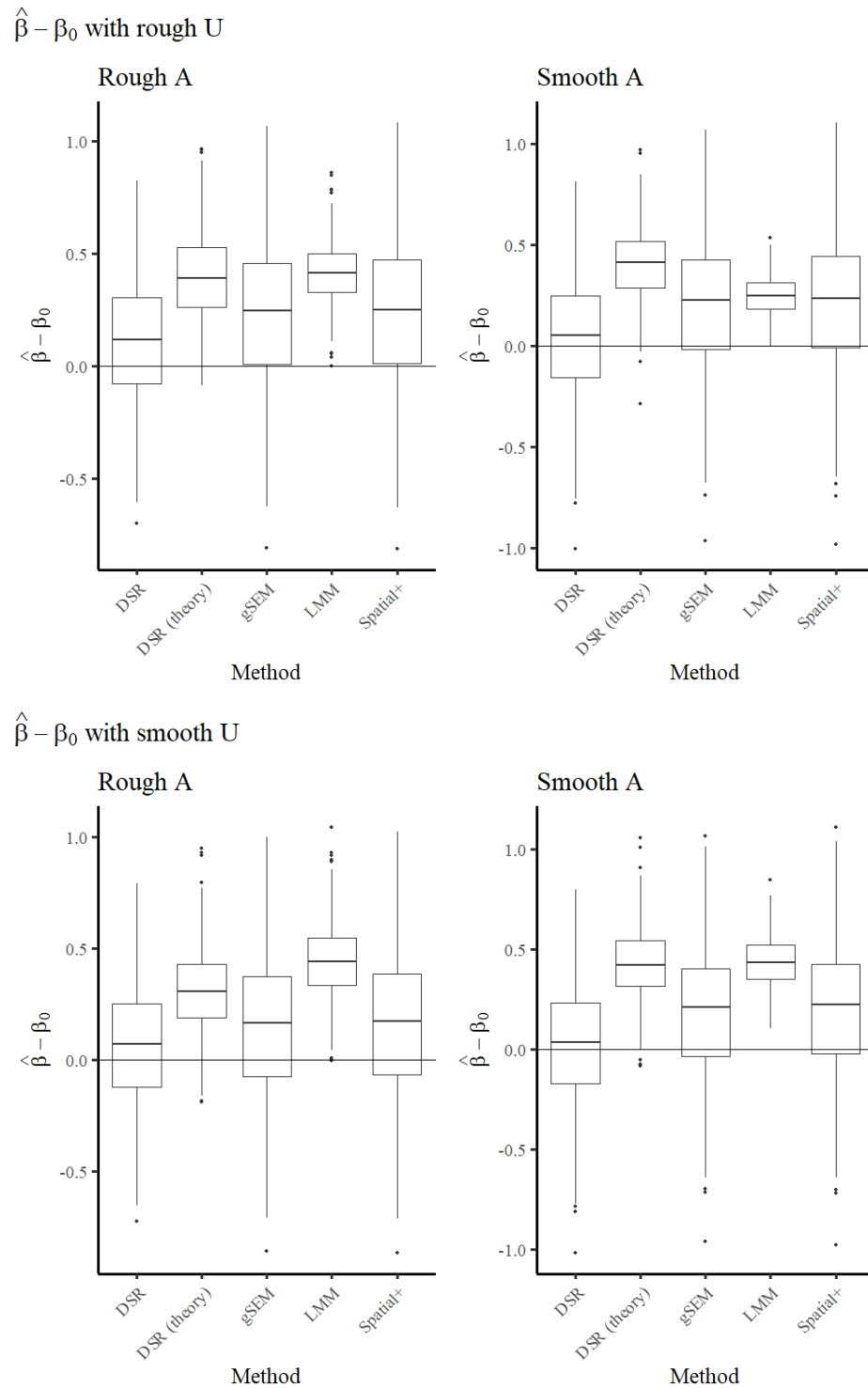


Figure 1: Sampling distribution of $\hat{\beta} - \beta_0$ from DSR, theoretical DSR, gSEM, LMM, and Spatial+. On the left side, the unobserved confounder U is smooth, while on the right side it is rough. The smoothness of the treatment variable A is similarly varied.

Table S1: Coverage (mean confidence interval length) of 95% confidence intervals for DSR, theoretical DSR, gSEM, LMM, and Spatial+ in illustrative scenarios. Scenarios varied by the smoothness of the treatment variable A and the unobserved spatial confounder U .

A	U	DSR	Theoretical DSR	gSEM	LMM	Spatial+
Rough	Rough	0.92 (1.14)	0.56 (0.84)	0.94 (1.54)	0.13 (0.51)	0.95 (1.59)
Smooth	Rough	0.97 (1.30)	0.47 (0.78)	0.94 (1.55)	0.24 (0.35)	0.95 (1.62)
Rough	Smooth	0.94 (1.15)	0.71 (0.84)	0.97 (1.54)	0.23 (0.64)	0.97 (1.59)
Smooth	Smooth	0.98 (1.36)	0.45 (0.79)	0.95 (1.55)	0.07 (0.46)	0.95 (1.62)

Table S2: Summary statistics of treatment and response variables used in the analysis of PFAS exposure's association with TSH in 98 women from the private well community near the Fayetteville fluorochemical plant.

Variable	Median	Mean	SD
PFHpS (ng/mL)	0.31	0.47	0.60
PFHxS (ng/mL)	1.96	2.34	1.58
PFNA (ng/mL)	0.55	0.68	0.54
PFOS (ng/mL)	5.87	7.02	5.16
PFOA (ng/mL)	2.17	2.50	1.79
TSH (uIU/mL)	1.34	1.51	0.71

Table S3: Slope estimates, t-values (subscript) and standard errors (in parentheses) for the multi-exposure model. Methods are ordinary least-squares (OLS), spatial linear mixed model (LMM), double spatial regression (DSR), and geoadditve structural equation model (gSEM).

Variable	OLS	LMM	DSR	gSEM
PFNA	0.07 _{0.55} (0.13)	0.11 _{0.96} (0.12)	0.10 _{0.79} (0.13)	0.09 _{0.54} (0.17)
PFOA	0.02 _{0.66} (0.03)	0.02 _{0.83} (0.03)	0.03 _{1.00} (0.03)	0.01 _{0.17} (0.04)
PFOS	-0.04 _{-2.56} (0.01)	-0.04 _{-3.36} (0.01)	-0.04 _{-3.14} (0.01)	-0.03 _{-2.27} (0.01)
PFHpS	-0.02 _{-0.20} (0.10)	-0.10 _{-1.18} (0.08)	-0.13 _{-1.80} (0.07)	-0.10 _{-0.72} (0.14)
PFHxS	0.05 _{1.24} (0.04)	0.05 _{1.26} (0.08)	0.05 _{1.32} (0.04)	0.06 _{1.36} (0.05)

Table S4: Slope estimates, t-values (subscript) and standard errors (in parentheses) for the single-exposure model. Results from DSR analyzing association between one PFAS at a time and $\log(\text{TSH})$.

Variable	DSR
PFNA	0.01 _{0.10} (0.11)
PFOA	0.00 _{0.23} (0.03)
PFOS	-0.02 _{-2.40} (0.01)
PFHpS	-0.13 _{-1.89} (0.07)
PFHxS	0.01 _{0.36} (0.04)

Table S5: Simulation results for rough **U** and rough **A**. Metrics are bias, relative bias (bias divided by β_0), mean squared error (MSE), confidence interval (CI) length, coverage (CVG), and power. CI length, coverage, and power are computed with respect to 95% confidence intervals.

	Bias	Rel. Bias	MSE	CI Length	CVG	Power
OLS	0.502	1.004	0.348	0.199	0.075	0.998
LMM	0.416	0.832	0.192	0.512	0.125	1.000
Spline (GCV)	0.406	0.812	0.185	0.552	0.190	1.000
Spline (REML)	0.410	0.820	0.188	0.540	0.175	1.000
Spatial+	0.234	0.468	0.170	1.595	0.948	0.432
gSEM	0.228	0.455	0.165	1.541	0.935	0.462
DSR (theory)	0.399	0.799	0.200	0.838	0.555	0.990
DSR (theory, no crossfit)	0.394	0.787	0.202	0.921	0.630	0.983
DSR	0.112	0.224	0.092	1.139	0.915	0.552
DSR (no crossfit)	0.113	0.227	0.091	1.132	0.917	0.552
DSR (spline)	0.136	0.271	0.088	1.051	0.917	0.652
DSR (alt., spline)	0.228	0.455	0.165	1.308	0.885	0.568

Table S6: Simulation results for rough \mathbf{U} and smooth \mathbf{A} . Metrics are bias, relative bias (bias divided by β_0), mean squared error (MSE), confidence interval (CI) length, coverage (CVG), and power. CI length, coverage, and power are computed with respect to 95% confidence intervals.

	Bias	Rel. Bias	MSE	CI Length	CVG	Power
OLS	0.363	0.726	0.177	0.166	0.085	1.000
LMM	0.249	0.498	0.070	0.352	0.235	1.000
Spline (GCV)	0.236	0.471	0.064	0.352	0.278	1.000
Spline (REML)	0.236	0.472	0.064	0.342	0.252	1.000
Spatial+	0.222	0.444	0.169	1.619	0.945	0.415
gSEM	0.209	0.417	0.159	1.552	0.940	0.430
DSR (theory)	0.406	0.812	0.194	0.783	0.470	0.998
DSR (theory, no crossfit)	0.402	0.804	0.208	0.889	0.578	0.978
DSR	0.044	0.088	0.099	1.302	0.965	0.410
DSR (no crossfit)	0.050	0.099	0.092	1.249	0.973	0.445
DSR (spline)	0.109	0.217	0.057	0.835	0.907	0.792
DSR (alt., spline)	0.209	0.417	0.159	1.335	0.885	0.550

Table S7: Simulation results for smooth **U** and rough **A**. Metrics are bias, relative bias (bias divided by β_0), mean squared error (MSE), confidence interval (CI) length, coverage (CVG), and power. CI length, coverage, and power are computed with respect to 95% confidence intervals.

	Bias	Rel. Bias	MSE	CI Length	CVG	Power
OLS	0.522	1.043	0.356	0.215	0.060	1.000
LMM	0.443	0.887	0.225	0.637	0.232	1.000
Spline (GCV)	0.475	0.951	0.262	0.702	0.260	1.000
Spline (REML)	0.466	0.932	0.253	0.713	0.280	1.000
Spatial+	0.162	0.324	0.141	1.594	0.965	0.352
gSEM	0.153	0.307	0.135	1.541	0.965	0.360
DSR (theory)	0.315	0.631	0.137	0.843	0.705	0.983
DSR (theory, no crossfit)	0.290	0.579	0.130	0.918	0.785	0.943
DSR	0.067	0.133	0.085	1.146	0.940	0.492
DSR (no crossfit)	0.072	0.144	0.085	1.137	0.940	0.507
DSR (spline)	0.106	0.211	0.083	1.052	0.920	0.590
DSR (alt., spline)	0.153	0.307	0.135	1.290	0.910	0.522

Table S8: Simulation results for smooth **U** and smooth **A**. Metrics are bias, relative bias (bias divided by β_0), mean squared error (MSE), confidence interval (CI) length, coverage (CVG), and power. CI length, coverage, and power are computed with respect to 95% confidence intervals.

	Bias	Rel. Bias	MSE	CI Length	CVG	Power
OLS	0.498	0.997	0.291	0.174	0.028	1.000
LMM	0.434	0.869	0.206	0.461	0.065	1.000
Spline (GCV)	0.435	0.870	0.208	0.463	0.075	1.000
Spline (REML)	0.431	0.862	0.204	0.477	0.088	1.000
Spatial+	0.210	0.419	0.163	1.619	0.950	0.398
gSEM	0.194	0.388	0.151	1.552	0.950	0.412
DSR (theory)	0.431	0.862	0.216	0.790	0.448	1.000
DSR (theory, no crossfit)	0.392	0.784	0.194	0.886	0.610	0.988
DSR	0.029	0.057	0.099	1.364	0.975	0.370
DSR (no crossfit)	0.047	0.094	0.092	1.294	0.963	0.420
DSR (spline)	0.180	0.359	0.080	0.840	0.828	0.858
DSR (alt., spline)	0.194	0.388	0.151	1.320	0.887	0.545

Table S9: Simulation results for middle-out heteroskedastic errors. Metrics are bias, relative bias (bias divided by β_0), mean squared error (MSE), confidence interval (CI) length, coverage (CVG), and power. CI length, coverage, and power are computed with respect to 95% confidence intervals.

	Bias	Rel. Bias	MSE	CI Length	CVG	Power
OLS	0.165	0.329	0.036	0.106	0.102	1.000
LMM	0.151	0.301	0.027	0.236	0.310	1.000
Spline (GCV)	0.151	0.302	0.028	0.266	0.428	1.000
Spline (REML)	0.152	0.304	0.028	0.252	0.380	1.000
Spatial+	0.162	0.325	0.087	1.139	0.948	0.632
gSEM	0.149	0.298	0.081	1.089	0.950	0.637
DSR (theory)	0.220	0.441	0.063	0.550	0.667	1.000
DSR (theory, no crossfit)	0.221	0.443	0.073	0.622	0.713	0.993
DSR	0.016	0.033	0.048	0.889	0.963	0.637
DSR (no crossfit)	0.022	0.044	0.044	0.845	0.955	0.665
DSR (spline)	0.062	0.123	0.027	0.585	0.938	0.940
DSR (alt., spline)	0.149	0.298	0.081	0.934	0.900	0.760

Table S10: Simulation results for cubed confounder. Metrics are bias, relative bias (bias divided by β_0), mean squared error (MSE), confidence interval (CI) length, coverage (CVG), and power. CI length, coverage, and power are computed with respect to 95% confidence intervals.

	Bias	Rel. Bias	MSE	CI Length	CVG	Power
OLS	1.449	2.899	3.164	0.426	0.025	1.000
LMM	0.465	0.929	0.292	1.029	0.557	0.925
Spline (GCV)	0.558	1.115	0.398	1.021	0.455	0.970
Spline (REML)	0.466	0.931	0.294	1.069	0.598	0.927
Spatial+	0.114	0.228	0.141	1.638	0.980	0.285
gSEM	0.077	0.155	0.119	1.552	0.978	0.282
DSR (theory)	0.935	1.869	1.175	1.163	0.192	0.990
DSR (theory, no crossfit)	0.747	1.494	0.767	1.162	0.330	0.980
DSR	0.071	0.142	0.112	1.268	0.925	0.442
DSR (no crossfit)	0.088	0.176	0.112	1.207	0.897	0.502
DSR (spline)	0.263	0.526	0.158	0.798	0.680	0.882
DSR (alt., spline)	0.077	0.155	0.119	1.254	0.925	0.448

Table S11: Simulation results for gamma-distributed errors. Metrics are bias, relative bias (bias divided by β_0), mean squared error (MSE), confidence interval (CI) length, coverage (CVG), and power. CI length, coverage, and power are computed with respect to 95% confidence intervals.

	Bias	Rel. Bias	MSE	CI Length	CVG	Power
OLS	0.416	0.832	0.210	0.166	0.055	1.000
LMM	0.367	0.733	0.151	0.429	0.108	1.000
Spline (GCV)	0.364	0.728	0.151	0.452	0.148	1.000
Spline (REML)	0.364	0.729	0.151	0.450	0.142	1.000
Spatial+	0.199	0.398	0.158	1.619	0.963	0.385
gSEM	0.184	0.368	0.148	1.552	0.960	0.400
DSR (theory)	0.390	0.780	0.183	0.790	0.500	0.995
DSR (theory, no crossfit)	0.367	0.734	0.178	0.890	0.635	0.978
DSR	0.022	0.044	0.099	1.341	0.973	0.382
DSR (no crossfit)	0.039	0.079	0.091	1.271	0.963	0.408
DSR (spline)	0.150	0.299	0.072	0.834	0.858	0.835
DSR (alt., spline)	0.184	0.368	0.148	1.323	0.890	0.530

Table S12: Simulation results for east-west heteroskedastic errors. Metrics are bias, relative bias (bias divided by β_0), mean squared error (MSE), confidence interval (CI) length, coverage (CVG), and power. CI length, coverage, and power are computed with respect to 95% confidence intervals.

	Bias	Rel. Bias	MSE	CI Length	CVG	Power
OLS	0.250	0.499	0.078	0.150	0.072	1.000
LMM	0.230	0.461	0.062	0.331	0.230	1.000
Spline (GCV)	0.230	0.461	0.063	0.369	0.320	1.000
Spline (REML)	0.232	0.464	0.063	0.351	0.282	1.000
Spatial+	0.195	0.389	0.156	1.618	0.960	0.382
gSEM	0.182	0.365	0.147	1.552	0.948	0.388
DSR (theory)	0.350	0.700	0.151	0.783	0.603	0.993
DSR (theory, no crossfit)	0.339	0.677	0.162	0.887	0.715	0.975
DSR	0.014	0.028	0.096	1.293	0.973	0.400
DSR (no crossfit)	0.024	0.048	0.089	1.233	0.965	0.422
DSR (spline)	0.092	0.184	0.053	0.832	0.907	0.780
DSR (alt., spline)	0.182	0.365	0.147	1.333	0.895	0.520

Table S13: Simulation results for $\sigma_A^2 = 1$. Metrics are bias, relative bias (bias divided by β_0), mean squared error (MSE), confidence interval (CI) length, coverage (CVG), and power. CI length, coverage, and power are computed with respect to 95% confidence intervals. Note that Shift (BART) results are included, without variance estimates.

	Bias	Rel. Bias	MSE	CI Length	CVG	Power
OLS	0.232	0.464	0.065	0.121	0.070	1.000
LMM	0.025	0.050	0.002	0.124	0.855	1.000
Spline (GCV)	0.027	0.054	0.002	0.124	0.858	1.000
Spline (REML)	0.024	0.049	0.002	0.124	0.870	1.000
Spatial+	0.020	0.041	0.001	0.161	0.978	1.000
gSEM	0.003	0.005	0.001	0.165	0.988	1.000
Shift (Bart)	-0.002	-0.005	0.002	-	-	-
DSR (theory)	0.012	0.023	0.001	0.124	0.930	1.000
DSR (theory, no crossfit)	0.008	0.016	0.001	0.124	0.932	1.000
DSR	0.009	0.018	0.001	0.115	0.925	1.000
DSR (no crossfit)	0.010	0.020	0.001	0.115	0.920	1.000
DSR (spline)	0.009	0.018	0.001	0.115	0.920	1.000
DSR (alt., spline)	0.003	0.005	0.001	0.123	0.945	1.000

Table S14: Simulation results for very rough, exponential spatial processes generating \mathbf{U} and \mathbf{A} . Metrics are bias, relative bias (bias divided by β_0), mean squared error (MSE), confidence interval (CI) length, coverage (CVG), and power. CI length, coverage, and power are computed with respect to 95% confidence intervals.

	Bias	Rel. Bias	MSE	CI Length	CVG	Power
OLS	0.501	1.003	0.279	0.174	0.005	1.000
LMM	0.485	0.971	0.241	0.274	0.000	1.000
Spline (GCV)	0.483	0.966	0.239	0.294	0.000	1.000
Spline (REML)	0.486	0.972	0.242	0.273	0.000	1.000
Spatial+	0.611	1.222	0.389	0.605	0.010	1.000
gSEM	0.591	1.183	0.366	0.600	0.015	1.000
DSR (theory)	0.493	0.985	0.250	0.325	0.000	1.000
DSR (theory, no crossfit)	0.549	1.098	0.317	0.356	0.002	1.000
DSR	0.459	0.919	0.223	0.377	0.010	1.000
DSR (no crossfit)	0.460	0.919	0.223	0.376	0.010	1.000
DSR (spline)	0.462	0.923	0.223	0.380	0.007	1.000
DSR (alt., spline)	0.591	1.183	0.366	0.460	0.007	1.000

Table S15: Simulation results for spatial locations located on a regular grid. Metrics are bias, relative bias (bias divided by β_0), mean squared error (MSE), confidence interval (CI) length, coverage (CVG), and power. CI length, coverage, and power are computed with respect to 95% confidence intervals.

	Bias	Rel. Bias	MSE	CI Length	CVG	Power
OLS	0.488	0.975	0.277	0.171	0.030	1.000
LMM	0.431	0.863	0.205	0.442	0.075	1.000
Spline (GCV)	0.430	0.859	0.205	0.444	0.085	1.000
Spline (REML)	0.428	0.855	0.203	0.455	0.095	1.000
Spatial+	0.215	0.430	0.167	1.596	0.945	0.390
gSEM	0.199	0.398	0.155	1.529	0.940	0.415
DSR (theory)	0.435	0.869	0.221	0.767	0.378	1.000
DSR (theory, no crossfit)	0.398	0.797	0.203	0.866	0.578	0.993
DSR	0.021	0.043	0.102	1.379	0.970	0.338
DSR (no crossfit)	0.025	0.050	0.101	1.374	0.970	0.340
DSR (spline)	0.180	0.360	0.081	0.817	0.828	0.853
DSR (alt., spline)	0.199	0.398	0.155	1.300	0.887	0.550

Table S16: Simulation results for deterministic latent functions of space g_0 and m_0 such that $g_0 = m_0$. Metrics are bias, relative bias (bias divided by β_0), mean squared error (MSE), confidence interval (CI) length, coverage (CVG), and power. CI length, coverage, and power are computed with respect to 95% confidence intervals.

	Bias	Rel. Bias	MSE	CI Length	CVG	Power
OLS	0.959	1.919	0.924	0.244	0.000	1.000
LMM	0.957	1.913	0.919	0.252	0.000	1.000
Spline (GCV)	0.956	1.913	0.919	0.252	0.000	1.000
Spline (REML)	0.958	1.917	0.922	0.247	0.000	1.000
Spatial+	0.227	0.454	0.170	1.600	0.953	0.428
gSEM	0.208	0.416	0.156	1.521	0.938	0.450
DSR (theory)	0.576	1.152	0.388	0.997	0.350	0.990
DSR (theory, no crossfit)	0.486	0.971	0.314	1.089	0.593	0.948
DSR	0.227	0.455	0.140	1.086	0.825	0.693
DSR (no crossfit)	0.295	0.590	0.152	0.981	0.750	0.855
DSR (spline)	0.371	0.743	0.181	0.874	0.603	0.963
DSR (alt., spline)	0.208	0.416	0.156	1.304	0.892	0.580

Table S17: Simulation results for deterministic latent functions of space g_0 and m_0 such that $g_0 \neq m_0$. Metrics are bias, relative bias (bias divided by β_0), mean squared error (MSE), confidence interval (CI) length, coverage (CVG), and power. CI length, coverage, and power are computed with respect to 95% confidence intervals.

	Bias	Rel. Bias	MSE	CI Length	CVG	Power
OLS	0.987	1.974	0.979	0.271	0.000	1.000
LMM	0.873	1.746	0.769	0.511	0.000	1.000
Spline (GCV)	0.844	1.688	0.722	0.541	0.000	1.000
Spline (REML)	0.849	1.698	0.729	0.538	0.000	1.000
Spatial+	0.195	0.390	0.156	1.600	0.965	0.395
gSEM	0.176	0.352	0.143	1.521	0.960	0.418
DSR (theory)	0.529	1.058	0.334	1.003	0.430	0.985
DSR (theory, no crossfit)	0.401	0.802	0.228	1.088	0.693	0.925
DSR	0.159	0.318	0.101	1.124	0.905	0.645
DSR (no crossfit)	0.238	0.475	0.119	0.993	0.825	0.812
DSR (spline)	0.333	0.666	0.161	0.836	0.618	0.958
DSR (alt., spline)	0.176	0.352	0.143	1.298	0.892	0.542